

A MULTIPLICATIVE-NOISE MECHANISM FOR VARIABILITY AMPLIFICATION UNDER RADIATIVE FORCING IN AN ARCTIC ENERGY-BALANCE MODEL

GIANMARCO DEL SARTO, FRANCO FLANDOLI, AND MARTA LENZI

ABSTRACT. We propose and analyse a mechanism by which CO₂-driven radiative forcing can increase Arctic temperature variability in a stochastic Sellers-type energy-balance model. Starting from a fast-slow formulation in which insolation is modelled by a rapidly mean-reverting Ornstein-Uhlenbeck process while temperature evolves on a slow macroweather timescale, a Wong-Zakai reduction leads to a stochastic energy-balance equation with *multiplicative* noise. After linearising around the stable equilibrium $T^{*,\lambda}$, we derive an explicit expression for the stationary variance of the temperature anomaly and prove that it increases monotonically with the forcing parameter λ whenever $T^{*,\lambda}$ lies in the ice-sensitive regime of the co-albedo. We then consider a spatial anomaly model and its finite-difference semi-discretisation, obtaining a finite-dimensional SDE. Under natural stability conditions and nonnegative noise correlations, we establish a component-wise monotone increase of the stationary covariance matrix with respect to λ , including its off-diagonal entries. In particular, radiative forcing amplifies not only local variances but also the covariance between temperature anomalies at distinct spatial locations, indicating increased similarity in the variability of the anomaly field across space.

CONTENTS

Introduction	1
1. Radiative forcing amplifies variance in a multiplicative-noise 0D-EBM	3
1.1. Preliminaries: energy balance models and Wong-Zakai principle	3
1.2. Fast-slow insolation-temperature model and reduction to a multiplicative-noise EBM	5
1.3. Stationary variance and monotone dependence on radiative forcing	7
2. Spatial anomaly model and finite-dimensional approximation	9
2.1. Spatial EBM with Dirichlet data and anomaly formulation	9
2.2. Finite-difference semi-discretisation	10
2.3. Stationary covariance for the semi-discrete anomaly SDE	12
2.4. Monotonicity of the stationary covariance in the radiative forcing parameter	16
3. Analysis of observational sea surface temperature data	20
Acknowledgments	21
References	23

INTRODUCTION

Background and motivation. The Arctic is warming significantly faster than the global average, a phenomenon known as Arctic Amplification [50]. A primary driver of this process is the ice-albedo feedback: as snow and sea ice melt, the surface darkens and absorbs more shortwave radiation [27, 58]. Extreme events are controlled not only by shifts in the mean, but also by changes in variability. In particular, an increase in variance widens the distribution and makes persistent or extreme warm events more likely [29, 49]. This paper proposes and analyses, within a mathematically tractable framework, a mechanism by which CO₂-driven radiative forcing can *increase Arctic temperature variability* through the temperature-dependent ice-albedo feedback.

Modelling framework and main results. We work within the class of energy balance models (EBMs), an elementary class of climate models [42]. In their simplest form, EBMs describe the evolution of a representative near-surface temperature through the balance between absorbed shortwave radiation and emitted longwave radiation [7, 23, 48]. EBMs are appreciated for their mathematical tractability [15, 16, 21, 22], and for capturing key mechanisms driving Earth’s climate [5, 8, 14, 25]. A central ingredient in Sellers-type EBMs is a *Lipschitz* co-albedo function $\beta(T)$ encoding the reduction of albedo with warming as sea ice and snow retreat [36, 41, 45]. This co-albedo nonlinearity is the simplest representation of the ice-albedo feedback and is known to generate multiple regimes and tipping-like behaviour in low-order climate models [3, 24, 38]. In the present paper, rather than focusing on regime shifts, we address how radiative forcing modifies the *stationary variance and covariance* of temperature anomalies around a stable equilibrium.

A standard approach to modelling unresolved “weather” variability in climate dynamics is to introduce stochastic forcing, in the spirit of Hasselmann-type stochastic climate models [2, 28, 57]. In EBMs, noise is often assumed to be additive. However, this is a simplifying assumption, as already pointed out in the Hasselmann programme, where the correct form of the noise is the *multiplicative* one [28]. This motivates our starting point: a fast-slow formulation in which insolation (or a proxy) evolves on a fast “weather” timescale (e.g. one day) while temperature evolves on a slow macroweather timescale (e.g. one year). A related fast-slow insolation–temperature setup was recently considered in [37]; here we focus on the reduction to a closed equation for the slow variable and the resulting monotone variance/covariance amplification.

More precisely, we consider a coupled fast-slow system in which insolation is modelled by a rapidly mean-reverting Ornstein-Uhlenbeck process with correlation time $\tau \ll 1$, while temperature obeys a radiative balance law with co-albedo feedback. We prove that the integrated fast fluctuations converge to Brownian motion as $\tau \rightarrow 0$. Since the integrated forcing is smooth for fixed $\tau > 0$, this naturally leads to a Wong-Zakai reduction: replacing the smooth driver by its Brownian limit yields a stochastic EBM with *multiplicative noise*. This provides a derivation which links fast weather variability to a reduced stochastic climate model with state-dependent noise.

Our main results quantify a forcing-induced *variance amplification mechanism* in this setting. After linearising the reduced multiplicative-noise EBM around a stable equilibrium $T^{*,\lambda}$ (depending on the radiative forcing parameter λ), we obtain an explicit formula for the stationary variance of the temperature anomaly. We then prove that this stationary variance increases monotonically with λ whenever $T^{*,\lambda}$ lies in the *ice-sensitive* regime of the co-albedo (i.e. where β has positive slope). The mechanism is clear. Increasing radiative forcing shifts the equilibrium temperature upward; in the ice-sensitive regime the co-albedo is increasing, so the effective amplitude of multiplicative noise and its impact on the anomaly dynamics increase accordingly, leading to higher stationary variance.

We then move from a single temperature variable to a spatial model that accounts for horizontal heat transport. We study the temperature anomaly around a reference equilibrium profile and approximate the resulting stochastic dynamics on a grid. This leads to a finite-dimensional stochastic model for the anomaly field, for which we can analyse the long-time covariance explicitly. Under standard stability assumptions and non-negative noise correlations, we show that increasing radiative forcing increases the stationary covariance matrix component-wise, and hence increases the stationary spatial variance (its trace), which we use as a second-moment proxy for fluctuation intensity and for the likelihood of large anomalies. This covariance-amplification prediction is complementary to recent harmonic-domain statistical approaches for time-dependent temperature fields on the sphere, where changes (or nonstationarity) in the dependence structure are investigated via the time evolution of spherical-harmonic coefficients and related change-point/structural-break methodology; see [9, 10, 39, 40].

Applicability and limitations. Our results are conditional on the existence of a stable deterministic temperature equilibrium $T^{*,\lambda}$ around which we linearise and compute stationary second moments. For Arctic applications this assumption is not automatic: it is essentially guaranteed in polar winter (when mean insolation is close to zero), but it can be questionable if the forcing is interpreted as summer or annual-mean, when the ice-albedo feedback is strongest. We nevertheless adopt stability as a first-order working

hypothesis, since key EBM parameters are uncertain and hard to calibrate regionally (i.e. in our Arctic setting), and because a more complete treatment would incorporate seasonality by prescribing a periodically time-dependent insolation. This would lead to a non-autonomous problem where the reference equilibrium $T^{*,\lambda}(t)$ (time dependent) describes a seasonal cycle rather than a fixed equilibrium. We leave this extension to future work.

Observational comparison. In the last part of the paper we compare our theoretical results with observations, asking whether the model-predicted variability changes can be seen in real data. Since the ice-albedo feedback is expected to be strongest when the mean state lies near the melt-sensitive temperature range, we focus on August *sea surface temperature* in the Arctic and adjacent northern high latitudes and track changes in both the mean and variability over the satellite era. More generally, variance changes under warming can depend strongly on the region [35]; here this suggests that variability changes should be spatially non-uniform, with Arctic seas and transition zones behaving differently from persistently ice-covered or warm open-ocean areas.

Organisation of the paper. This paper is organised as follows. Section 1 introduces the stochastic Sellers-type EBM, derives the multiplicative-noise reduced model via a fast-slow formulation and Wong-Zakai, and proves monotone variance amplification with respect to radiative forcing. Section 2 formulates the spatial anomaly model, constructs a finite difference semi-discretisation, derives covariance dynamics and its stationary limit, and establishes monotonicity of the stationary covariance and spatial variance under suitable assumptions. Lastly, Section 3 compares the model predictions with observational August *sea surface temperature* from the National Oceanic and Atmospheric Administration (NOAA) north of 60°N. We track temporal variability with moving decadal statistics and spatial heterogeneity with the within-region standard deviation, contrasting Arctic seas with regions showing little change.

1. RADIATIVE FORCING AMPLIFIES VARIANCE IN A MULTIPLICATIVE-NOISE 0D-EBM

1.1. Preliminaries: energy balance models and Wong-Zakai principle.

1.1.1. *Energy balance climate models.* Among the lowest-complexity levels in the climate-model hierarchy lie the class of *energy balance models* [42]. Introduced independently by Budyko and Sellers in 1969 [7, 48], EBMs describe the evolution of a representative (near-surface) temperature T (in Kelvin) through the balance between absorbed shortwave radiation \mathcal{R}_a and emitted longwave radiation \mathcal{R}_e . In its zero-dimensional form, the EBM is given by

$$(1.1) \quad C_{\text{eff}} \frac{dT}{dt} = \mathcal{R}_a - \mathcal{R}_e,$$

where $C_{\text{eff}} > 0$ is an effective heat capacity per unit area; equivalently, upon rescaling time one may set $C_{\text{eff}} = 1$ and recover $\frac{dT}{dt} = \mathcal{R}_a - \mathcal{R}_e$. The model can be enriched by incorporating a spatial variable (typically latitude, after zonal averaging) and representing meridional heat transport by diffusion, which yields a nonlinear parabolic PDE, see [23, 41].

In this work we adopt a reduced, regionally EBM for the Arctic. This choice is motivated by the fact that Arctic temperature variability and trends are strongly constrained by the local radiative energy budget and amplified by cryospheric feedbacks, most notably the sea-ice/snow albedo feedback, which makes reduced energy-balance descriptions informative at regional scales [17, 56]. Consistently, low-order energy-balance and sea-ice models have been adapted for recent studies for sea-ice stability, Arctic warming and ice-loss transitions [19, 25, 46].

For the emitted radiation \mathcal{R}_e we use the classical Budyko empirical formula [7, 42] and assume

$$\mathcal{R}_e(T) = r_0 + r_1 T,$$

with $r_0 \in \mathbb{R}$ and $r_1 > 0$. For the absorbed shortwave radiation we set

$$\mathcal{R}_a(T, Q, \lambda) = Q\beta(T) + \lambda,$$

where Q denotes the (possibly regionally averaged) incoming solar flux and $\beta \in (0, 1)$ is the *co-albedo*, i.e. the fraction of incident shortwave radiation absorbed ($\beta = 1 - \alpha$, with α the albedo). Here, as in [5, 13], λ

models the effect of greenhouse gases on the radiation balance; the larger is λ , the larger is the radiative forcing, and thus the greenhouse effect which leads to a higher absorbed radiation. Following continuous piece-wise linear parametrisation in the EBM literature as in [45], we consider

$$(1.2) \quad \beta(T) = \begin{cases} \beta_{\min}, & \text{if } T \leq T_l, \\ \beta_{\min} + \frac{\beta_{\max} - \beta_{\min}}{T_u - T_l}(T - T_l), & \text{if } T_l < T < T_u, \\ \beta_{\max}, & \text{if } T \geq T_u. \end{cases}$$

where β_{\min} and β_{\max} represent the limiting co-albedo values in, respectively, the ice-covered (cold) and ice-free (warm) regimes; typical values in Sellers-type models are $\beta_{\min} \approx 0.38$ and $\beta_{\max} \approx 0.70$ [41]. Here, $T_l = 263$ K and $T_u = 300$ K as in [45]. We emphasise that these values are not meant to represent the melting temperature of ice, but rather to parametrise the temperature range over which the *effective* (regionally averaged) ice cover, and hence the co-albedo, transitions from its ice-covered to its ice-free limit [41, 45]. This interpretation is consistent with the thermodynamics of melting. Since the phase change involves the latent heat of fusion, a large amount of energy is required to melt the ice, and the temperature can remain close to the freezing point while melting proceeds. In simple sea-ice/EBM formulations this ‘‘latent-heat buffering’’ is captured by treating melt in terms of an enthalpy (energy) budget when ice is present, see [18, 19]. Lastly, note that our EBM is of Sellers-type, meaning that the co-albedo is Lipschitz continuous. The other main class of EBMs is the Budyko type, which is characterised by a discontinuous co-albedo. In the latter case, it is known that uniqueness may fail; see, for example, [16] for a discussion of non-uniqueness of weak solutions.

1.1.2. *Wong-Zakai principle.* It is worth recalling the Wong-Zakai principle, a tool that we will use in Section 1.2. Roughly speaking, it asserts that if we consider smooth approximations W_t^ε of a Brownian motion W_t such that

$$W_t^\varepsilon \rightarrow W_t$$

in a sufficiently strong sense, then the solution Z_t^ε of the corresponding (pathwise deterministic, for fixed ω) differential equation

$$\frac{dZ_t^\varepsilon}{dt} = b(t, Z_t^\varepsilon) + \sigma(t, Z_t^\varepsilon) \frac{dW_t^\varepsilon}{dt},$$

converges (in the same mode of convergence as $W_t^\varepsilon \rightarrow W_t$), as $\varepsilon \rightarrow 0$, to the solution of the SDE driven by *Stratonovich noise*

$$dZ_t = b(t, Z_t) dt + \sigma(t, Z_t) \circ dW_t.$$

See, for instance, [32, Chapter 5.2] or [31, 55] for more details on the Wong-Zakai principle.

For the sake of clarity, we recall that the Stratonovich stochastic integral $\int_0^t \sigma(s, Z_s) \circ dW_s$ is defined as the limit (in probability) of Riemann sums using midpoint evaluation,

$$\sum_k \sigma \left(t_k, \frac{Z_{t_k} + Z_{t_{k+1}}}{2} \right) (W_{t_{k+1}} - W_{t_k}),$$

whenever the limit exists. This contrasts with the Itô integral $\int_0^t \sigma(s, Z_s) dW_s$, which is defined via left-point evaluation $\sigma(t_k, Z_{t_k})$. A key consequence is that Stratonovich calculus obeys the classical chain rule (as in ordinary calculus), while Itô calculus involves an additional quadratic-variation correction term. Concretely, for sufficiently regular coefficients one has the conversion formula

$$\int_0^t \sigma(s, Z_s) \circ dW_s = \int_0^t \sigma(s, Z_s) dW_s + \frac{1}{2} \int_0^t \partial_z \sigma(s, Z_s) \sigma(s, Z_s) ds,$$

so that an SDE written in Stratonovich form corresponds to an Itô SDE with an extra correction term in the drift term, see [47, Section 4.6].

1.2. Fast–slow insolation–temperature model and reduction to a multiplicative-noise EBM.

We consider a fast-slow system describing the interaction between a *slow* temperature process T evolving on a macroweather timescale (e.g. one year) and a *fast* component X evolving on a weather timescale (e.g. one day). In our setting, X represents (a proxy for) the insolation. We model X as a mean-reverting Ornstein-Uhlenbeck process fluctuating around a climatological mean level Q , while the temperature follows a radiative balance law. More precisely, on the slow time variable t we consider

$$(1.3) \quad \begin{cases} dX_t^\tau = -\frac{1}{\tau}(X_t^\tau - Q)dt + \frac{1}{\sqrt{\tau}}dW_t, & X_0^\tau = x_0, \\ \frac{dT_t^{\tau,\lambda}}{dt} = X_t^\tau\beta(T_t^{\tau,\lambda}) + \lambda - (r_0 + r_1T_t^{\tau,\lambda}), & T_0^{\tau,\lambda} = \theta_0, \end{cases}$$

where $(W_t)_t$ denotes a Brownian motion, and x_0, θ_0 are the deterministic initial conditions. The parameter $\tau > 0$ represents the ratio of the fast and slow timescales (e.g. $\tau \approx 1/365$ if the slow scale is one year and the fast one is one day). Even if τ is small, it is not infinitesimal in applications; this will be important in what follows.

A key feature of the scaling in (1.3) is that the variance of the invariant measure for X^τ does not depend on τ : indeed, for the OU process $dX_t^\tau = -(1/\tau)(X_t^\tau - Q)dt + (1/\sqrt{\tau})dW_t$ the stationary law is Gaussian with mean Q and variance $1/2$. Thus τ controls the *correlation time* of X^τ , not its variance.

At this point, we would like to deduce a closed equation for the slow process $T_t^{\tau,\lambda}$.

Lemma 1.1. *For any $t > 0$, it holds*

$$\lim_{\tau \rightarrow 0} \mathbb{E} \left| \frac{1}{\sqrt{\tau}} \int_0^t X_s^\tau ds - \frac{Qt}{\sqrt{\tau}} - W_t \right|^2 = 0.$$

Proof. For simplicity, we drop the dependence on τ in X^τ . The fast process X_t can be written explicitly as

$$\begin{aligned} X_t &= x_0 e^{-t/\tau} + \frac{1}{\tau} \int_0^t Q e^{-(t-s)/\tau} ds + \frac{1}{\sqrt{\tau}} \int_0^t e^{-(t-s)/\tau} dW_s \\ &= x_0 e^{-t/\tau} + Q \left(1 - e^{-t/\tau}\right) + \frac{1}{\sqrt{\tau}} \int_0^t e^{-(t-s)/\tau} dW_s \\ &= (x_0 - Q) e^{-t/\tau} + Q + \frac{1}{\sqrt{\tau}} \int_0^t e^{-(t-s)/\tau} dW_s. \end{aligned}$$

Thus, integrating in time, we get

$$\begin{aligned} \int_0^t X_s ds &= \int_0^t \left[(x_0 - Q) e^{-s/\tau} + Q + \frac{1}{\sqrt{\tau}} \int_0^s e^{-(s-r)/\tau} dW_r \right] ds \\ &= \tau \left(1 - e^{-t/\tau}\right) (x_0 - Q) + tQ + \frac{1}{\sqrt{\tau}} \int_0^t \int_0^s e^{-(s-r)/\tau} dW_r ds. \end{aligned}$$

The last term on the right-hand side (RHS) can be computed applying Fubini-Tonelli for stochastic integrals

$$\begin{aligned} \frac{1}{\sqrt{\tau}} \int_0^t \int_0^s e^{-(s-r)/\tau} dW_r ds &= \frac{1}{\sqrt{\tau}} \int_0^t \int_r^t e^{-(s-r)/\tau} ds dW_r = \sqrt{\tau} \int_0^t \left(1 - e^{-(t-r)/\tau}\right) dW_r \\ &= \sqrt{\tau} \left(W_t - \int_0^t e^{-(t-r)/\tau} dW_r \right). \end{aligned}$$

From the previous computations, we deduce

$$\begin{aligned}
\mathbb{E} \left| \frac{1}{\sqrt{\tau}} \int_0^t X_s ds - \frac{Qt}{\sqrt{\tau}} - W_t \right|^2 &= \mathbb{E} \left| \sqrt{\tau} \left(1 - e^{-t/\tau} \right) (x_0 - Q) - \int_0^t e^{-(t-r)/\tau} dW_r \right|^2 \\
&\leq 2\tau \left(1 - e^{-t/\tau} \right)^2 (x_0 - Q)^2 + 2\mathbb{E} \left| \int_0^t e^{-(t-r)/\tau} dW_r \right|^2 \\
&= 2\tau \left(1 - e^{-t/\tau} \right)^2 (x_0 - Q)^2 + 2 \int_0^t e^{-2(t-r)/\tau} dr \\
&= 2\tau \left(1 - e^{-t/\tau} \right)^2 (x_0 - Q)^2 + \tau \left(1 - e^{-2t/\tau} \right)
\end{aligned}$$

where the first inequality follows from the Jensen's inequality, and the following inequality by Itô-isometry. Taking the limits in τ , we conclude the proof. \square

Define the centred, integrated fast fluctuations

$$W_t^\tau := \frac{1}{\sqrt{\tau}} \int_0^t (X_s^\tau - Q) ds.$$

Since X^τ has continuous paths, W^τ is C^1 and

$$dW_t^\tau = \frac{1}{\sqrt{\tau}} (X_t^\tau - Q) dt.$$

Lemma 1.1 yields $W_t^\tau \rightarrow W_t$ in L^2 for each fixed t . Using this identity, the temperature equation in (1.3) can be rewritten as the random ODE

$$(1.4) \quad dT_t^{\tau,\lambda} = \left(Q\beta(T_t^{\tau,\lambda}) + \lambda - \mathcal{R}_e(T_t^{\tau,\lambda}) \right) dt + \sqrt{\tau} \beta(T_t^{\tau,\lambda}) dW_t^\tau,$$

where the last integral is understood pathwise (Riemann-Stieltjes), since W^τ is C^1 . We now invoke the Wong–Zakai principle (see Section 1.1). Since (1.4) is driven by the smooth process W^τ , replacing W^τ by its Brownian limit W leads to a Stratonovich interpretation of the limiting stochastic integral. Accordingly, for $\tau \ll 1$ we approximate $T^{\tau,\lambda}$ by the solution $\tilde{T}^{\tau,\lambda}$ of

$$(1.5) \quad d\tilde{T}_t^{\tau,\lambda} = \left(Q\beta(\tilde{T}_t^{\tau,\lambda}) + \lambda - \mathcal{R}_e(\tilde{T}_t^{\tau,\lambda}) \right) dt + \sqrt{\tau} \beta(\tilde{T}_t^{\tau,\lambda}) \circ dW_t.$$

In Itô form, (1.5) becomes

$$(1.6) \quad d\tilde{T}_t^{\tau,\lambda} = \left(Q\beta(\tilde{T}_t^{\tau,\lambda}) + \lambda - \mathcal{R}_e(\tilde{T}_t^{\tau,\lambda}) + \frac{\tau}{2} \beta(\tilde{T}_t^{\tau,\lambda}) \beta'(\tilde{T}_t^{\tau,\lambda}) \right) dt + \sqrt{\tau} \beta(\tilde{T}_t^{\tau,\lambda}) dW_t.$$

We stress that we are not taking a literal limit $\tau \rightarrow 0$ from (1.4) to (1.5). Doing so would indeed make the diffusion coefficient vanish. Rather, τ is the (small but positive) ratio between the fast and slow time scales, and the passage from (1.4) to (1.5) is a *model reduction step*: for $\tau \ll 1$, the forcing generated by the fast OU process is approximated by a white-noise forcing, with Stratonovich interpretation suggested by Wong–Zakai.

We study fluctuations near the stable equilibrium $T^{*,\lambda}$, so the *temperature anomaly*

$$Y_t^{\tau,\lambda} := \tilde{T}_t^{\tau,\lambda} - T^{*,\lambda}$$

stays small and it is natural to linearise $\beta(T)$ around $T^{*,\lambda}$. The Itô–Stratonovich correction is an $O(\tau)$ drift term, and since $\tau \approx 1/365$ (with β, β' bounded) it is much smaller than the remaining deterministic drift modelling the radiation balance $\mathcal{R}_a - \mathcal{R}_e$. So we can neglect it. Thus, we define $T^{*,\lambda}$ as the stable equilibrium temperature $T^* = T^{*,\lambda}$ of the deterministic stationary equation associated to (1.6). We stress that it is an assumption of our analysis that $T^{*,\lambda}$ is a stable equilibrium point for the deterministic EBM (1.1). In other words, $T^{*,\lambda}$ is solution of

$$(1.7) \quad Q\beta(T^{*,\lambda}) + \lambda - \mathcal{R}_e(T^{*,\lambda}) = 0,$$

and it is (locally asymptotically) stable for the deterministic dynamics, i.e. the linearisation of $\frac{dT}{dt} = Q\beta(T) + \lambda - \mathcal{R}_e(T)$ at $T^{*,\lambda}$ has negative slope

$$\frac{d}{dT}(Q\beta(T) + \lambda - \mathcal{R}_e(T))|_{T=T^{*,\lambda}} = Q\beta'(T^{*,\lambda}) - \mathcal{R}'_e(T^{*,\lambda}) < 0,$$

equivalently

$$(1.8) \quad b^\lambda = \mathcal{R}'_e(T^{*,\lambda}) - Q\beta'(T^{*,\lambda}) > 0$$

Since β is piecewise linear by (1.2), for T in a neighbourhood of $T^{*,\lambda}$ that does not cross T_l or T_u we have the affine representation

$$(1.9) \quad \beta(T) = \beta(T^{*,\lambda}) + \beta'(T^{*,\lambda})(T - T^{*,\lambda}),$$

with $\beta'(T^{*,\lambda}) = 0$ outside (T_l, T_u) and $\beta'(T^{*,\lambda}) = (\beta_{\max} - \beta_{\min})/(T_u - T_l)$ inside. Thus, recalling that $\mathcal{R}_e(T) = r_0 + r_1T$ is already linear, we get, applying (1.9) in (1.6) and using (1.7) to cancel the constant drift,

$$(1.10) \quad dY_t^{\tau,\lambda} = (Q\beta'(T^{*,\lambda}) - r_1) Y_t^{\tau,\lambda} dt + \sqrt{\tau} \left(\beta(T^{*,\lambda}) + \beta'(T^{*,\lambda}) Y_t^{\tau,\lambda} \right) dW_t, \quad Y_0 = y_0,$$

where y_0 is some deterministic initial condition. Introducing the shorthands

$$b^\lambda := -Q\beta'(T^{*,\lambda}) + r_1, \quad \sigma_0^\lambda := \beta(T^{*,\lambda}), \quad \sigma_1^\lambda := \beta'(T^{*,\lambda}),$$

then the linear EBM (1.10) assumes the compact form

$$dY_t^{\tau,\lambda} = -b^\lambda Y_t^{\tau,\lambda} dt + \sqrt{\tau}(\sigma_0^\lambda + \sigma_1^\lambda Y_t^{\tau,\lambda}) dW_t, \quad Y_0^{\tau,\lambda} = y_0.$$

Remark 1.2 (On the stability condition (1.8)). *Condition (1.8) is the stability requirement for the deterministic EBM at $T^{*,\lambda}$. It is automatic outside the ice-sensitive range (i.e. $T^{*,\lambda} < T_l$ or $T^{*,\lambda} > T_u$) because $\beta'(T^{*,\lambda}) = 0$ and thus $b^\lambda = r_1 > 0$. In the ice-sensitive range (i.e. $T^{*,\lambda} \in (T_l, T_u)$) the sign of $b^\lambda = r_1 - Q\beta'(T^{*,\lambda})$ depends on the magnitude of Q . For an Arctic winter mean, we can reasonably consider $Q \approx 0$; so stability is expected. On the other hand, for summer or annual-mean forcing the condition can fail. Since our stationary-variance analysis requires a stable linearisation, we treat (1.8) as an explicit modelling assumption delimiting the regime of validity. A more realistic approach would introduce seasonal forcing $Q = Q(t)$, yielding a non-autonomous model; we leave this for future work.*

1.3. Stationary variance and monotone dependence on radiative forcing. In this section we prove that the stationary variance associated to the solution of (1.10) increases monotonically with respect to λ . This means that, as the CO₂ concentration in the atmosphere increases, the same holds for the variance of the climate, i.e. the stationary temperature anomaly.

We start by observing that, since $t \mapsto \int_0^t (\sigma_0^\lambda + \sigma_1^\lambda Y_s^{\tau,\lambda}) dW_s$ is a martingale, then the expected value of the process $Y_t^{\tau,\lambda}$ satisfies

$$(1.11) \quad \mathbb{E}[Y_t^{\tau,\lambda}] = y_0 - b^\lambda \int_0^t \mathbb{E}[Y_s^{\tau,\lambda}] ds.$$

This can be seen by writing (1.10) in the integral form and then considering the expectation. The solution of (1.11) is

$$\mathbb{E}[Y_t^{\tau,\lambda}] = e^{-b^\lambda t} y_0, \quad t \geq 0.$$

Thus the limit for large time t of the expected value of $Y_t^{\tau,\lambda}$ exists and it is independent of y_0 if and only if $b^\lambda > 0$. In that case, we have

$$\lim_{t \rightarrow +\infty} \mathbb{E}[Y_t^{\tau,\lambda}] = 0.$$

This motivates once more why the assumption $b^\lambda > 0$ from (1.8) is natural in this framework. Further, to simplify the computation, we also assume $y_0 = 0$, which gives $\mathbb{E}[Y_t^{\tau,\lambda}] = 0$ for any $t \geq 0$. The following result identifies the value of the stationary variance associated to the equation (1.10).

Proposition 1.3. *Assume*

$$b^\lambda > 0, \quad 2b^\lambda - \tau(\sigma_1^\lambda)^2 > 0.$$

Then the following limit exists

$$\lim_{t \rightarrow +\infty} \mathbb{E}[|Y_t^{\tau, \lambda}|^2] = \frac{\tau(\sigma_0^\lambda)^2}{2b^\lambda - \tau(\sigma_1^\lambda)^2}.$$

Proof. We drop the superscript τ, λ for readability. We assume for simplicity $y_0 = 0$ and use the notation $V(t) = \mathbb{E}[|Y_t|^2]$. Thus Y_t is a centered process. The Itô formula gives

$$\begin{aligned} d(Y_t)^2 &= 2Y_t dY_t + d[Y.]_t \\ (1.12) \quad &= 2Y_t (-bY_t dt + \sqrt{\tau}(\sigma_0 + \sigma_1 Y_t) dW_t) + \tau(\sigma_0 + \sigma_1 Y_t)^2 dt \\ &= [-(2b - \tau\sigma_1^2)Y_t^2 + 2\tau\sigma_0\sigma_1 Y_t + \tau\sigma_0^2] dt + dM_t, \end{aligned}$$

where $[Y.]_t$ denotes the quadratic variation of the process Y_t and M_t is a martingale. Considering the expected value in the previous equality, and using that $\mathbb{E}[Y_t] = 0$, yields

$$\frac{d}{dt} V(t) = -(2b - \tau\sigma_1^2)V(t) + \tau\sigma_0^2.$$

Since $V(0) = 0$, its solution is

$$V(t) = \tau\sigma_0^2 \int_0^t e^{-(2b - \tau\sigma_1^2)(t-s)} ds = \frac{\tau\sigma_0^2}{2b - \tau\sigma_1^2} \left(1 - e^{-(2b - \tau\sigma_1^2)t}\right).$$

Hence

$$\lim_{t \rightarrow +\infty} V(t) = \frac{\tau\sigma_0^2}{2b - \tau\sigma_1^2},$$

provided that $2b - \tau\sigma_1^2 > 0$. □

We are now ready to prove the main result of this section, which deals with the increase of the stationary variance under an increase of the radiative forcing, modelled by λ .

Proposition 1.4. *Assume*

$$b^\lambda > 0, \quad 2b^\lambda - \tau(\sigma_1^\lambda)^2 > 0, \quad T^{*, \lambda} \in (T_l, T_u).$$

Then the stationary variance is monotone increasing. In other words, setting

$$\lambda \mapsto \text{Var}_\infty(\lambda) := \lim_{t \rightarrow +\infty} \mathbb{E}[|Y_t^{\tau, \lambda}|^2] = \frac{\tau(\sigma_0^\lambda)^2}{2b^\lambda - \tau(\sigma_1^\lambda)^2} = \frac{\tau\beta(T^{*, \lambda})^2}{2(r_1 - Q\beta'(T^{*, \lambda})) - \tau\beta'(T^{*, \lambda})^2},$$

we have $\text{Var}_\infty(\lambda)' > 0$.

Proof. Assume for simplicity $y_0 = 0$. Recall that $T^{*, \lambda}$ is defined by

$$Q\beta(T^{*, \lambda}) + \lambda - \mathcal{R}_e(T^{*, \lambda}) = 0,$$

and that the linearised coefficients are

$$b^\lambda = r_1 - Q\beta'(T^{*, \lambda}), \quad \sigma_0^\lambda = \beta(T^{*, \lambda}), \quad \sigma_1^\lambda = \beta'(T^{*, \lambda}).$$

By Proposition 1.3, the stationary variance of the temperature anomaly $Y_t^{\tau, \lambda} = \tilde{T}_t^{\tau, \lambda} - T^{*, \lambda}$ is

$$\text{Var}_\infty(\lambda) = \lim_{t \rightarrow +\infty} \mathbb{E}[|Y_t^{\tau, \lambda}|^2] = \frac{\tau(\sigma_0^\lambda)^2}{2b^\lambda - \tau(\sigma_1^\lambda)^2} = \frac{\tau\beta(T^{*, \lambda})^2}{2(r_1 - Q\beta'(T^{*, \lambda})) - \tau\beta'(T^{*, \lambda})^2}.$$

Step 1: increasing λ increases the equilibrium temperature $T^{, \lambda}$.* Differentiating implicitly the equilibrium equation in λ gives

$$(Q\beta'(T^{*, \lambda}) - \mathcal{R}'_e(T^{*, \lambda})) \frac{dT^{*, \lambda}}{d\lambda} + 1 = 0.$$

Since $\mathcal{R}'_e(T) \equiv r_1$ and $b^\lambda = r_1 - Q\beta'(T^{*, \lambda})$, this becomes

$$\frac{dT^{*, \lambda}}{d\lambda} = \frac{1}{b^\lambda} > 0.$$

Step 2: monotone increase in stationary variance. For simplicity, set

$$N(\lambda) := \tau\beta(T^{*,\lambda})^2, \quad D(\lambda) := 2(r_1 - Q\beta'(T^{*,\lambda})) - \tau\beta'(T^{*,\lambda})^2$$

so that

$$\text{Var}_\infty(\lambda) = \frac{N(\lambda)}{D(\lambda)}.$$

In Step 1 we have proved that $\lambda \mapsto T^{*,\lambda}$ is monotone increasing. Further, the co-albedo β is increasing by the standard modelling of EBMs. Hence

$$(1.13) \quad N'(\lambda) = 2\tau\beta(T^{*,\lambda})\beta'(T^{*,\lambda})\frac{dT^{*,\lambda}}{d\lambda} > 0.$$

Note that $\beta'(T^{*,\lambda})$ is non-zero (and positive), since $T^{*,\lambda} \in (T_l, T_u)$, thanks to (1.2). Regarding $D(\lambda)$, since β is piece-wise linear, then $\beta'' = 0$. Hence

$$(1.14) \quad D'(\lambda) = -2\beta''(T^{*,\lambda})(Q + \tau\beta'(T^{*,\lambda}))\frac{dT^{*,\lambda}}{d\lambda} = 0.$$

Combining (1.13) and (1.14), we conclude that

$$\text{Var}'_\infty(\lambda) = \frac{N'(\lambda)D(\lambda) - N(\lambda)D'(\lambda)}{D(\lambda)^2} = \frac{N'(\lambda)D(\lambda)}{D(\lambda)^2} > 0,$$

since $D(\lambda) > 0$ thanks to the assumption $2b^\lambda - \tau(\sigma_1^\lambda)^2 > 0$. \square

The previous result indicates, in climate terms, that stronger CO₂ forcing not only warms the equilibrium states, but also that, via the ice-albedo feedback, amplifies the temperature anomaly around the equilibrium state. Indeed, the monotone increase of the stationary variance can be read directly from the explicit formula

$$\text{Var}_\infty(\lambda) = \frac{\tau\beta(T^{*,\lambda})^2}{2(r_1 - Q\beta'(T^{*,\lambda})) - \tau\beta'(T^{*,\lambda})^2}.$$

By Step 1 in the previous proof, increasing λ increases the equilibrium temperature $T^{*,\lambda}$. If $T^{*,\lambda} \in (T_l, T_u)$, then β is strictly increasing, hence the numerator $\tau\beta(T^{*,\lambda})^2$ increases with λ . Moreover, since β is affine on (T_l, T_u) , we have $\beta'(T^{*,\lambda}) \equiv (\beta_{\max} - \beta_{\min})/(T_u - T_l)$, so the denominator $2(r_1 - Q\beta'(T^{*,\lambda})) - \tau\beta'(T^{*,\lambda})^2$ is constant (in this regime). Therefore $\text{Var}_\infty(\lambda)$ increases with λ . In climate terms, stronger CO₂ forcing not only warms the equilibrium state, but also amplifies fluctuations around it via the temperature dependence of the co-albedo (ice-albedo feedback).

2. SPATIAL ANOMALY MODEL AND FINITE-DIMENSIONAL APPROXIMATION

In this section we extend the zero-dimensional stochastic energy balance model (1.6) from Section 1 to a space-dependent version, appropriate for a regional model (the Arctic). This is done by introducing horizontal heat transport. We first formulate in Section 2.1 an energy-balance SPDE with *multiplicative* noise, with Dirichlet non-homogeneous boundary data representing the influence of adjacent areas. In Section 2.2 we then construct a finite-difference semi-discretisation, obtaining a finite-dimensional SDE for the temperature anomaly. In Section 2.3 we derive the closed evolution equation for the covariance matrix of the SDE and identify its stationary limit. Finally, in Section 2.4 we prove that the stationary covariance increases (entry-wise) with the radiative forcing parameter λ , given natural assumptions on the covariance of the noise and the deterministic dynamics.

2.1. Spatial EBM with Dirichlet data and anomaly formulation. Let $\mathcal{D} \subset \mathbb{R}^2$ be a bounded domain with sufficiently regular boundary $\partial\mathcal{D}$. We consider a Hasselmann-type stochastic energy balance model with diffusion, i.e. the spatially dependent extension of equation (1.6). The (near-surface) temperature field $T^{\tau,\lambda}(t, x)$, depending on the time-scale parameter τ and the radiative forcing λ , satisfies non-homogeneous Dirichlet boundary conditions

$$(2.1) \quad T^{\tau,\lambda}(t, \xi) = \theta(\xi), \quad t \geq 0, \quad \xi \in \partial\mathcal{D},$$

where θ is a prescribed boundary profile; in the following, we assume θ to be independent of the radiative forcing parameter λ , but our analysis extends to the case of $\theta = \theta^\lambda$. On \mathcal{D} we postulate the Itô SPDE

$$(2.2) \quad \begin{cases} dT_t^{\tau,\lambda} = \left(\Delta T_t^{\tau,\lambda} + Q \beta(T_t^{\tau,\lambda}) + \lambda - \mathcal{R}_e(T_t^{\tau,\lambda}) \right) dt + \sqrt{\tau} \beta(T_t^{\tau,\lambda}) dW_t, \\ T^{\tau,\lambda}|_{\partial\mathcal{D}} = \theta \\ T^{\tau,\lambda}|_{t=0} = T_0 \end{cases}$$

where $Q = Q(x)$ denotes the given insolation function, β is the co-albedo, λ is the radiative forcing parameter, W_t is a Wiener process on $L^2(\mathcal{D})$, and T_0 is the initial condition. We do not specify the details of these objects here, as we use them only heuristically; the interested reader may consult [12].

Assume, for simplicity, that the Dirichlet datum θ is time-independent. We define the reference profile $T^{*,\lambda}$ as a (stable) stationary solution of the deterministic problem with the same boundary values

$$(2.3) \quad \begin{cases} \Delta T^{*,\lambda}(x) + Q(x) \beta(T^{*,\lambda}(x)) + \lambda - \mathcal{R}_e(T^{*,\lambda}(x)) = 0, & x \in \mathcal{D}, \\ T^{*,\lambda}(\xi) = \theta(\xi), & \xi \in \partial\mathcal{D}. \end{cases}$$

The temperature anomaly is then defined by

$$Y_t^{\tau,\lambda}(x) := T_t^{\tau,\lambda}(x) - T^{*,\lambda}(x).$$

By construction, (2.1) and (2.3) yield

$$(2.4) \quad Y_t^{\tau,\lambda}(\xi) = 0, \quad \xi \in \partial\mathcal{D},$$

i.e. the anomaly satisfies homogeneous Dirichlet boundary conditions. Subtracting (2.3) from (2.2) gives the anomaly SPDE

$$(2.5) \quad dY_t^{\tau,\lambda} = \left(\Delta Y_t^{\tau,\lambda} + Q(\beta(T^{*,\lambda} + Y_t^{\tau,\lambda}) - \beta(T^{*,\lambda})) - (\mathcal{R}_e(T^{*,\lambda} + Y_t^{\tau,\lambda}) - \mathcal{R}_e(T^{*,\lambda})) \right) dt + \sqrt{\tau} \beta(T^{*,\lambda} + Y_t^{\tau,\lambda}) dW_t,$$

with homogeneous Dirichlet boundary condition (2.4). As in the zero-dimensional case, if y is small, it holds the relation

$$\beta(T^{*,\lambda} + y) = \beta(T^{*,\lambda}) + \beta'(T^{*,\lambda}) y.$$

Since in our model \mathcal{R}_e is affine (e.g. $\mathcal{R}_e(T) = r_0 + r_1 T$), we obtain the linear multiplicative SPDE

$$(2.6) \quad \begin{cases} dY_t^{\tau,\lambda} = \left(\Delta Y_t^{\tau,\lambda} - a^\lambda Y_t^{\tau,\lambda} \right) dt + \sqrt{\tau} \left(\beta(T^{*,\lambda}) + \beta'(T^{*,\lambda}) Y_t^{\tau,\lambda} \right) dW_t, \\ Y^{\tau,\lambda}|_{\partial\mathcal{D}} = 0, \\ Y^{\tau,\lambda}|_{t=0} = T_0 - T^{*,\lambda}, \end{cases}$$

where

$$a^\lambda(x) := -Q(x) \beta'(T^{*,\lambda}(x)) + \mathcal{R}'_e(T^{*,\lambda}(x)).$$

Equation (2.6) is complemented with homogeneous Dirichlet boundary conditions (2.4). We are not interested in the well-posedness of (2.6) here; the SPDE is a formal starting point for the semi-discrete covariance analysis.

2.2. Finite-difference semi-discretisation. We now derive a finite-difference approximation of (2.6) on a two-dimensional mesh. For simplicity we present the construction on a rectangular grid; the resulting semi-discrete SDE has the same structure on general meshes, with A_Δ replaced by the corresponding stiffness matrix. We refer to [34, 44] for detailed treatments of finite difference methods for parabolic PDEs.

To describe the numerical discretisation, assume for simplicity $\mathcal{D} = (0, L_x) \times (0, L_y)$. Consider the uniform grid $x_i = ih_x$ for $i = 0, \dots, N_x$ and $y_j = jh_y$ for $j = 0, \dots, N_y$. We denote by

$$\mathcal{I} := \{1, \dots, N_x - 1\} \times \{1, \dots, N_y - 1\}$$

the set of interior index pairs, and by

$$z_{i,j} := (x_i, y_j) \in \mathcal{D}, \quad (i, j) \in \mathcal{I},$$

the corresponding interior grid points. We enumerate the interior nodes by a single index $m = 1, \dots, d$ (with $d = (N_x - 1)(N_y - 1)$) via the bijection

$$m = m(i, j) := (j - 1)(N_x - 1) + i, \quad (i, j) \in \mathcal{I},$$

and write $z_m := z_{i,j}$ whenever $m = m(i, j)$. Define the nodal unknowns $Y_{i,j}^{\tau,\lambda}(t) := Y_t^{\tau,\lambda}(z_{i,j})$ for $(i, j) \in \mathcal{I}$. Using the bijection $m = m(i, j)$, we collect these interior nodal values into the vector $Y_t^{\tau,\lambda} \in \mathbb{R}^d$, with $d = (N_x - 1)(N_y - 1)$, by setting $(Y_t^{\tau,\lambda})_m := Y_{i,j}^{\tau,\lambda}(t)$ whenever $m = m(i, j)$. The five-point stencil for the Laplacian at an interior node reads

$$(\Delta_h Y^{\tau,\lambda})_{i,j} = \frac{Y_{i+1,j}^{\tau,\lambda} - 2Y_{i,j}^{\tau,\lambda} + Y_{i-1,j}^{\tau,\lambda}}{h_x^2} + \frac{Y_{i,j+1}^{\tau,\lambda} - 2Y_{i,j}^{\tau,\lambda} + Y_{i,j-1}^{\tau,\lambda}}{h_y^2},$$

see [34, Section 3.2] for more details on the discretisation of the Laplace operator. Since $Y^{\tau,\lambda}$ satisfies homogeneous Dirichlet boundary conditions (2.4), boundary values are zero and no boundary forcing appears. In matrix form,

$$(2.7) \quad \Delta_h Y_t^{\tau,\lambda} = A_\Delta Y_t^{\tau,\lambda},$$

where

$$(2.8) \quad A_\Delta = \frac{1}{h_x^2} (I_{N_y-1} \otimes A_x) + \frac{1}{h_y^2} (A_y \otimes I_{N_x-1}),$$

and $A_x = \text{tridiag}(1, -2, 1) \in \mathbb{R}^{(N_x-1) \times (N_x-1)}$, $A_y = \text{tridiag}(1, -2, 1) \in \mathbb{R}^{(N_y-1) \times (N_y-1)}$. Define the sampled coefficients on interior nodes

$$b_m^\lambda := a^\lambda(z_m), \quad d_m^\lambda := \beta'(T^{*,\lambda}(z_m)), \quad f_m^\lambda := \beta(T^{*,\lambda}(z_m)), \quad m = 1, \dots, d.$$

Set

$$B^\lambda := \text{diag}(b^\lambda) \in \mathbb{R}^{d \times d}, \quad D^\lambda := \text{diag}(d^\lambda) \in \mathbb{R}^{d \times d}, \quad f^\lambda := (f_i^\lambda)_{i=1}^d \in \mathbb{R}^d.$$

To discretise the spatially correlated noise, let $C \in \mathbb{R}^{d \times d}$ be the discrete covariance matrix induced by the covariance operator of W on the grid, and fix a factorisation $C = LL^T$. Let $(W_t)_t$ be a d -dimensional Brownian motion. Then the semi-discrete approximation of (2.6) reads

$$(2.9) \quad dY_t^{\tau,\lambda} = (A_\Delta - B^\lambda)Y_t^{\tau,\lambda} dt + \sqrt{\tau} \text{diag}(D^\lambda Y_t^{\tau,\lambda} + f^\lambda) L dW_t, \quad Y^{\tau,\lambda}|_{t=0} = y_0.$$

We conclude this section by introducing a scalar proxy for the fluctuation level of the semi-discrete anomaly process (2.9), given by the trace of its covariance matrix. From now on, fix $\tau > 0$ and write $Y^\lambda := Y^{\tau,\lambda}$.

Definition 2.1 (Spatial Variance). *Let $(Y_t^\lambda)_t$ be the solution of the SDE (2.9) and let $\Gamma_t^\lambda := \mathbb{E}[(Y_t^\lambda - \mathbb{E}[Y_t^\lambda])(Y_t^\lambda - \mathbb{E}[Y_t^\lambda])^T]$ be its covariance matrix. The spatial variance at time t is*

$$\text{Var}_{\text{sp}}(t; \lambda) := \text{Tr}(\Gamma_t^\lambda),$$

and, whenever the limit exists, the stationary spatial variance is

$$\text{Var}_{\text{sp},\infty}(\lambda) := \text{Tr}(\Gamma_\infty^\lambda), \quad \Gamma_\infty^\lambda := \lim_{t \rightarrow \infty} \Gamma_t^\lambda.$$

In the discussion of spatial variance below we assume $y_0 = 0$. In the next subsection we briefly allow general y_0 to describe the mean, and then we set $y_0 = 0$ again to obtain an autonomous covariance equation. Thus, with the assumption $y_0 = 0$, from the fact that the drift is linear and the stochastic integral is a martingale, it follows that $\mathbb{E}[Y_t^\lambda] = 0$ for all $t \geq 0$. In this case,

$$\text{Var}_{\text{sp}}(t; \lambda) = \text{Tr}(\Gamma_t^\lambda) = \sum_{i=1}^d \text{Var}(Y_{t,i}^\lambda) = \mathbb{E} \left[\sum_{i=1}^d |Y_{t,i}^\lambda|^2 \right].$$

So $\text{Var}_{\text{sp}}(t; \lambda)$ is the sum of the local fluctuation intensities over the domain, and $\text{Var}_{\text{sp},\infty}(\lambda)$ measures this total variance in the stationary regime.

Remark 2.2 (Stationary spatial variance and extreme weather events). *It is natural to focus on the stationary spatial variance $\text{Var}_{\text{sp},\infty}(\lambda) = \text{Tr}(\Gamma_\infty^\lambda)$, since it measures the fluctuation level of the temperature anomaly in the long-time regime corresponding to the climate configuration determined by the radiative forcing λ (after transients have died out). In particular, comparing $\text{Var}_{\text{sp},\infty}(\lambda_1)$ and $\text{Var}_{\text{sp},\infty}(\lambda_2)$ quantifies how the typical amplitude of persistent spatial fluctuations changes when the forcing level (e.g. CO₂) is modified.*

Although extreme events are not determined by second moments alone, $\text{Var}_{\text{sp}}(t; \lambda)$ provides a useful second-moment control on the probability of observing a large anomaly somewhere in the domain. Assume for simplicity $y_0 = 0$, so that $\mathbb{E}[Y_t^\lambda] = 0$ for all $t \geq 0$. For any $\vartheta > 0$, by Markov's inequality

$$\mathbb{P}\left(\max_{1 \leq i \leq d} |Y_{t,i}^\lambda| \geq \vartheta\right) \leq \frac{1}{\vartheta^2} \mathbb{E}\left[\max_{1 \leq i \leq d} |Y_{t,i}^\lambda|^2\right] \leq \frac{1}{\vartheta^2} \mathbb{E}\left[\sum_{i=1}^d |Y_{t,i}^\lambda|^2\right] = \frac{\text{Var}_{\text{sp}}(t; \lambda)}{\vartheta^2}.$$

and the same estimate holds in the stationary regime with $\text{Var}_{\text{sp},\infty}(\lambda)$.

2.3. Stationary covariance for the semi-discrete anomaly SDE. Recall from Definition 2.1 that our scalar proxy for the fluctuation level is the spatial variance $\text{Var}_{\text{sp}}(t; \lambda) = \text{Tr}(\Gamma_t^\lambda)$ and its stationary limit $\text{Var}_{\text{sp},\infty}(\lambda) = \text{Tr}(\Gamma_\infty^\lambda)$ whenever it exists. Thus, establishing existence and monotonicity properties for Γ_∞^λ immediately yields corresponding results for $\text{Var}_{\text{sp},\infty}(\lambda)$.

2.3.1. Preliminaries: matrix order, M -matrices, and vectorisation. We collect a few standard facts that will be used to control the sign and monotonicity properties of the stationary covariance. For $A \in \mathbb{R}^{d \times d}$ we denote by $\rho(A)$ its spectral radius,

$$\rho(A) := \max\{|\mu| : \mu \text{ eigenvalue of } A\},$$

and we write $A \geq B$ for the component-wise order. Recall that a matrix A is a Z -matrix if $a_{ij} \leq 0$ for all $i \neq j$. A (non-singular) M -matrix is a Z -matrix of the form $A = sI - B$ with $B \geq 0$ and $s > \rho(B)$; equivalently, A is a Z -matrix with $\text{Re}(\mu) > 0$ for every eigenvalue μ , see [6, 43]. The key consequence we will use is the element-wise non-negativity of the inverse.

Theorem 2.3. *Let A be a Z -matrix. The following are equivalent:*

- (i) A is a non-singular M -matrix,
- (ii) $\text{Re}(\mu) > 0$ for every eigenvalue μ of A ,
- (iii) A is invertible and $A^{-1} \geq 0$ component-wise.

Second, we recall that an *irreducible matrix* A is a square matrix that cannot be transformed, via a permutation matrix P (specifically PAP^T), into a block upper triangular matrix with more than one diagonal block of positive size. Equivalently, A is irreducible if its associated directed graph is strongly connected. We refer to [6, Chapter 2.2.] for more details and properties on irreducible matrices

Finally, we fix notation for vectorisation and Kronecker products. Given $A = (v_1 | \dots | v_d) \in \mathbb{R}^{d \times d}$, we define

$$\text{vec}(A) := \begin{pmatrix} v_1 \\ \vdots \\ v_d \end{pmatrix} \in \mathbb{R}^{d^2}.$$

For matrices $A \in \mathbb{R}^{m \times n}$ and $B \in \mathbb{R}^{p \times q}$, we denote by $A \otimes B \in \mathbb{R}^{mp \times nq}$ their *Kronecker product*, defined blockwise by

$$A \otimes B := \begin{pmatrix} a_{11}B & \cdots & a_{1n}B \\ \vdots & \ddots & \vdots \\ a_{m1}B & \cdots & a_{mn}B \end{pmatrix}.$$

We will repeatedly use the identities

$$(2.10) \quad (A \otimes B)^T = A^T \otimes B^T, \quad \text{vec}(AXB) = (B^T \otimes A) \text{vec}(X),$$

as well as bilinearity in each argument.

2.3.2. *Covariance dynamics and Lyapunov-vectorised formulation.* In this subsection we derive the evolution equation satisfied by the covariance matrix of the semi-discrete anomaly process. By vectorising the resulting Lyapunov-type equation, we obtain a linear ODE in \mathbb{R}^{d^2} , whose long-time limit gives an explicit representation of the stationary covariance.

First, observe that SDE (2.9) can be rewritten as

$$dY_t^\lambda = M^\lambda Y_t^\lambda dt + \Sigma^\lambda(Y_t^\lambda) dW_t, \quad Y^\lambda|_{t=0} = y_0.$$

with $M^\lambda := A_\Delta - B^\lambda$ and $\Sigma^\lambda(y) = \sqrt{\tau} \text{diag}(D^\lambda y + f^\lambda)L$. Then the expected value $\mathbb{E}[Y_t^\lambda]$ satisfies

$$\frac{d}{dt} \mathbb{E}[Y_t^\lambda] = M^\lambda \mathbb{E}[Y_t^\lambda], \quad \mathbb{E}[Y_0^\lambda] = y_0$$

The solution is

$$\mathbb{E}[Y_t^\lambda] = e^{M^\lambda t} y_0.$$

It is reasonable, as in Section 1.3, that the temperature anomaly goes to zero as $t \rightarrow +\infty$. This holds for any initial condition y_0 if M^λ is negative definite, an assumption that we will always adopt from now on.

We are interested in the covariance matrix

$$\Gamma_t^\lambda := \mathbb{E}[(Y_t^\lambda - \mathbb{E}[Y_t^\lambda])(Y_t^\lambda - \mathbb{E}[Y_t^\lambda])^T].$$

For general y_0 , the covariance dynamics contain an additional (time-dependent) forcing term through $\mathbb{E}[Y_t^\lambda] = e^{M^\lambda t} y_0$. To keep the covariance equation autonomous and simplify the subsequent vectorised Lyapunov formulation, we impose the simplifying assumption $y_0 = 0$, so that $\mathbb{E}[Y_t^\lambda] = 0$ for all $t \geq 0$ and thus $\Gamma_t^\lambda = \mathbb{E}[Y_t^\lambda (Y_t^\lambda)^T]$.

Lemma 2.4. *Assume that $M^\lambda = A_\Delta - B^\lambda$ is negative definite and $y_0 = 0$. Then Γ_t^λ satisfies the matrix ODE*

$$\begin{aligned} \frac{d}{dt} \Gamma_t^\lambda &= M^\lambda \Gamma_t^\lambda + \Gamma_t^\lambda (M^\lambda)^T + \mathbb{E}[\Sigma^\lambda(Y_t^\lambda) (\Sigma^\lambda(Y_t^\lambda))^T] \\ &= M^\lambda \Gamma_t^\lambda + \Gamma_t^\lambda (M^\lambda)^T + \tau \sum_{k=1}^d \text{diag}(l^k) (D^\lambda \Gamma_t^\lambda (D^\lambda)^T + f^\lambda (f^\lambda)^T) \text{diag}(l^k), \end{aligned}$$

where l^k is the k -th column of L .

Proof. Assume for simplicity $\tau = 1$. We drop for the ease of notation the dependence on λ . Using Itô-formula

$$\begin{aligned} d(Y_t Y_t^T) &= (dY_t)(Y_t)^T + Y_t (dY_t)^T + (dY_t)(dY_t)^T \\ &= (MY_t dt + \Sigma dW_t)(Y_t)^T + Y_t (MY_t dt + \Sigma dW_t)^T + (dY_t)(dY_t)^T. \end{aligned}$$

Note that, using Itô isometry, we have

$$(dY_t)(dY_t)^T = (MY_t dt + \Sigma dW_t)(MY_t dt + \Sigma dW_t)^T = \Sigma dW_t (dW_t)^T \Sigma^T.$$

Since $dW_t (dW_t)^T = Idt$, we obtain

$$(dY_t)(dY_t)^T = \Sigma \Sigma^T dt.$$

In conclusion we have

$$d(Y_t Y_t^T) = [MY_t (Y_t)^T + Y_t (Y_t)^T M^T + \Sigma \Sigma^T] dt + \widetilde{M}_t,$$

where \widetilde{M}_t denotes a martingale. Taking the expected values, we deduce

$$\frac{d}{dt} \Gamma_t = M \Gamma_t + \Gamma_t M^T + \mathbb{E}[\Sigma \Sigma^T].$$

But in our setting $\Sigma = \text{diag}(DY_t + f)L$, thus

$$\Sigma \Sigma^T = \text{diag}(DY_t + f) L L^T \text{diag}(DY_t + f)^T.$$

Since

$$LL^T = \sum_{k=1}^d l^k (l^k)^T,$$

we obtain

$$\Sigma \Sigma^T = \sum_{k=1}^d \text{diag}(DY_t + f) l^k (l^k)^T \text{diag}(DY_t + f)^T,$$

Further, using the property

$$\text{diag}(a)b = \text{diag}(b)a, \quad a, b \in \mathbb{R}^d,$$

we have

$$\Sigma \Sigma^T = \sum_{k=1}^d \text{diag}(l^k) [(DY_t + f)(DY_t + f)^T] \text{diag}(l^k).$$

Since $\mathbb{E}[Y_t] = 0$, we have

$$\mathbb{E}[(DY_t + f)(DY_t + f)^T] = D\Gamma_t D^T + f f^T,$$

and thus

$$\mathbb{E}[\Sigma \Sigma^T] = \sum_{k=1}^d \text{diag}(l^k) (D\Gamma_t D^T + f f^T) \text{diag}(l^k).$$

□

In the following technical result, we write the ODE satisfied by the covariance matrix Γ_t in more tractable way.

Lemma 2.5. *Assume that $M^\lambda = A_\Delta - B^\lambda$ is negative definite and $y_0 = 0$. The ODE for Γ_t^λ*

$$\frac{d}{dt} \Gamma_t^\lambda = M^\lambda \Gamma_t^\lambda + \Gamma_t^\lambda (M^\lambda)^T + \tau \sum_{k=1}^d \text{diag}(l^k) (D^\lambda \Gamma_t^\lambda (D^\lambda)^T + f^\lambda (f^\lambda)^T) \text{diag}(l^k),$$

is equivalent to

$$(2.11) \quad \frac{d}{dt} q_t^\lambda = K^\lambda q_t^\lambda + F^\lambda,$$

with

$$q_t^\lambda = \text{vec}(\Gamma_t^\lambda), \quad K^\lambda := I_d \otimes M^\lambda + M^\lambda \otimes I_d + \tau \text{diag}(\text{vec}(C)) (D^\lambda \otimes D^\lambda),$$

and

$$F^\lambda = \tau \text{diag}(\text{vec}(C)) \text{vec}(f^\lambda (f^\lambda)^T),$$

Proof. Assume for simplicity $\tau = 1$. We drop the dependence on λ for the ease of notation. Consider the matrix ODE

$$\frac{d}{dt} \Gamma_t = M \Gamma_t + \Gamma_t M^T + \sum_{k=1}^d \text{diag}(l^k) (D \Gamma_t D^T + f f^T) \text{diag}(l^k).$$

Vectorising both sides gives

$$\frac{d}{dt} q_t = \text{vec}(M \Gamma_t) + \text{vec}(\Gamma_t M^T) + \sum_{k=1}^d \text{vec}(\text{diag}(l^k) (D \Gamma_t D^T + f f^T) \text{diag}(l^k)).$$

By the Kronecker product property (2.10),

$$\text{vec}(M \Gamma_t) = (I \otimes M) q_t, \quad \text{vec}(\Gamma_t M^T) = (M \otimes I) q_t.$$

For the noise term, again by (2.10), since $\text{diag}(l^k)^T = \text{diag}(l^k)$,

$$\text{vec}(\text{diag}(l^k) X \text{diag}(l^k)) = (\text{diag}(l^k) \otimes \text{diag}(l^k)) \text{vec}(X), \quad X \in \mathbb{R}^{d \times d}.$$

Apply this with $X = D\Gamma_t D^T + ff^T$ to obtain

$$\sum_{k=1}^d \text{vec}(\text{diag}(l^k)(D\Gamma_t D^T + ff^T)\text{diag}(l^k)) = \left(\sum_{k=1}^d \text{diag}(l^k) \otimes \text{diag}(l^k) \right) \text{vec}(D\Gamma_t D^T + ff^T).$$

Finally,

$$\text{vec}(D\Gamma_t D^T) = (D \otimes D) \text{vec}(\Gamma_t) = (D \otimes D) q_t, \quad \text{vec}(ff^T) \text{ is constant.}$$

Finally, since $C = LL^T$ and l^k denotes the k -th column of L , we have

$$\sum_{k=1}^d \text{diag}(l^k) \otimes \text{diag}(l^k) = \text{diag}(\text{vec}(C)),$$

because the (i, j) entry of C is $C_{ij} = \sum_{k=1}^d l_i^k l_j^k$, and vectorisation turns entrywise multiplication by C into multiplication by $\text{diag}(\text{vec}(C))$. Collecting terms yields

$$\frac{d}{dt} q_t = (I_d \otimes M + M \otimes I_d + \text{diag}(\text{vec}(C))(D \otimes D)) q_t + \text{diag}(\text{vec}(C)) \text{vec}(ff^T),$$

which is (2.11). \square

Combining the covariance identity from the previous lemma with the vectorisation rule in Lemma 2.5, we reduce the matrix-valued covariance dynamics to the linear ODE (2.11) on $q_t^\lambda = \text{vec}(\Gamma_t^\lambda)$; this directly gives the existence and an explicit formula for the stationary covariance under the hypothesis that K is negative-definite, and $C = LL^T$ is non-negative entry-wise.

Corollary 2.6. *Assume that $M^\lambda = A_\Delta - B^\lambda$ is negative definite, $y_0 = 0$ and*

$$K^\lambda = I_d \otimes M^\lambda + M^\lambda \otimes I_d + \tau \text{diag}(\text{vec}(C))(D^\lambda \otimes D^\lambda)$$

is negative definite. Assume further that $C = LL^T \geq 0$ component-wise. Then $\lim_{t \rightarrow \infty} \Gamma_t^\lambda =: \Gamma_\infty^\lambda$ exists. Further, setting $q^\lambda = \text{vec}(\Gamma_\infty^\lambda)$, we have

$$q^\lambda = (-K^\lambda)^{-1} F^\lambda,$$

Moreover $(-K^\lambda)^{-1} \geq 0$ component-wise.

Proof. Assume for simplicity $\tau = 1$. We drop the dependence on λ for the ease of notation. The first part of the statement consists in observing that the solution of the ODE (2.11) converges if K is negative definite.

Let's now check that, if K is negative definite, then $(-K)^{-1} \geq 0$ component-wise. Write

$$-K = I_d \otimes (-M) + (-M) \otimes I_d - \text{diag}(\text{vec}(C))(D \otimes D).$$

We claim that $-K$ is a Z -matrix, i.e. it has non-positive off-diagonal elements.

First, observe that $-M$ is a Z -matrix. Indeed, the discrete Laplacian A_Δ has non-negative off-diagonal entries and B is diagonal, hence $M = A_\Delta - B$ has non-negative off-diagonals. Therefore $-M$ has non-positive off-diagonals, i.e. $-M$ is a Z -matrix.

Second, both Kronecker products $I_d \otimes (-M)$ and $(-M) \otimes I_d$ have the same sign pattern off-diagonal as $-M$, therefore each of them is a Z -matrix. The same holds for their sum

Third, the term $\text{diag}(\text{vec}(C))(D \otimes D)$ is diagonal and non-negative. Indeed, since D is diagonal, then $D \otimes D$ is diagonal. Hence $\text{diag}(\text{vec}(C))(D \otimes D)$ is diagonal as well. Moreover, $C \geq 0$ entry-wise implies $\text{diag}(\text{vec}(C)) \geq 0$ entry-wise; therefore $\text{diag}(\text{vec}(C))(D \otimes D)$ has non-negative diagonal entries. Consequently, $\text{diag}(\text{vec}(C))(D \otimes D)$ only affects the diagonal of $-K$ and does not change any off-diagonal sign.

In conclusion, we have proved that $-K$ is a Z -matrix. By the hypothesis on K , we have that $-K$ is positive definite. By Theorem 2.3, we deduce that $(-K)^{-1} \geq 0$ component-wise. \square

2.4. Monotonicity of the stationary covariance in the radiative forcing parameter. We now study how the stationary covariance of the semi-discrete temperature anomaly depends on the forcing parameter λ . For each λ , let $Y_t^\lambda \in \mathbb{R}^d$ solve the finite-difference SDE (2.9) with $y_0 = 0$, i.e.

$$dY_t^\lambda = M^\lambda Y_t^\lambda dt + \sqrt{\tau} \text{diag}(D^\lambda Y_t^\lambda + f^\lambda) L dW_t, \quad Y_0^\lambda = 0,$$

where

$$M^\lambda := A_\Delta - B^\lambda, \quad B^\lambda := \text{diag}(b^\lambda), \quad D^\lambda := \text{diag}(d^\lambda), \quad f^\lambda \in \mathbb{R}^d, \quad C := LL^T.$$

Recall that the coefficients are obtained by sampling the equilibrium profile $T^{*,\lambda}$ on the interior grid points z_m :

$$(2.12) \quad b_m^\lambda = a^\lambda(z_m) = -Q(z_m)\beta'(T^{*,\lambda}(z_m)) + r_1, \quad d_m^\lambda = \beta'(T^{*,\lambda}(z_m)), \quad f_m^\lambda = \beta(T^{*,\lambda}(z_m)).$$

Here we used the affine form $\mathcal{R}_e(T) = r_0 + r_1 T$ so that $\mathcal{R}'_e(T) \equiv r_1$. Recall that, under the non-restrictive assumption $y_0 = 0$,

$$\Gamma_t^\lambda = \mathbb{E}[Y_t^\lambda (Y_t^\lambda)^T], \quad \Gamma_\infty^\lambda = \lim_{t \rightarrow \infty} \Gamma_t^\lambda,$$

whenever the limit exists. By Lemma 2.5 and Corollary 2.6, under the stability assumptions on M^λ and K^λ we have

$$q_\infty^\lambda := \text{vec}(\Gamma_\infty^\lambda) = (-K^\lambda)^{-1} F^\lambda,$$

where

$$(2.13) \quad F^\lambda = \tau \text{diag}(\text{vec}(C)) \text{vec}(f^\lambda (f^\lambda)^T).$$

As in the zero-dimensional case, one expects $\lambda \mapsto T^{*,\lambda}(x)$ to be increasing for each $x \in \mathcal{D}$ (see Section 1). Since, for $T \in (T_l, T_u)$, β is increasing, this implies that $\lambda \mapsto f^\lambda$ is increasing component-wise.

To control the λ -dependence of $B^\lambda = \text{diag}(b^\lambda)$ and $D^\lambda = \text{diag}((\beta'(T^{*,\lambda}(x_i)))_i)$, we assume, as above, that the equilibrium temperatures remain in a regime where β is increasing, e.g.

$$(2.14) \quad T^{*,\lambda}(z_m) \in (T_l, T_u), \quad m = 1, \dots, d,$$

so that $\partial_\lambda b^\lambda = 0$ and $\beta'(T^{*,\lambda}) \equiv \frac{\beta_{\max} - \beta_{\min}}{T_u - T_l}$.

Proposition 2.7 (Strict component-wise increase of the stationary covariance). *Let*

$$s := \frac{\beta_{\max} - \beta_{\min}}{T_u - T_l} > 0.$$

Assume that, for every λ under consideration, the equilibrium profile satisfies

$$T^{*,\lambda}(x) \in (T_l, T_u) \quad \text{for all } x \in \mathcal{D},$$

so that $\beta'(T^{,\lambda}(x)) \equiv s$ on \mathcal{D} . Assume moreover the coercivity condition*

$$(2.15) \quad r_1 - Q(x)s \geq 0 \quad \text{in } \mathcal{D}.$$

Let $C = LL^T$ and assume

$$C \geq 0 \text{ entry-wise}, \quad C \neq 0.$$

Assume that K^λ is negative definite, where

$$M^\lambda := A_\Delta - B^\lambda, \quad K^\lambda := I_d \otimes M^\lambda + M^\lambda \otimes I_d + \tau \text{diag}(\text{vec}(C)) (D^\lambda \otimes D^\lambda).$$

Then $\partial_\lambda \Gamma_\infty^\lambda > 0$ entry-wise.

Proof. Step 1: $\partial_\lambda T^{,\lambda} > 0$ in the interior.* Set $u^\lambda := \partial_\lambda T^{*,\lambda}$. Differentiating the elliptic equilibrium problem (2.3) with respect to λ yields

$$\Delta u^\lambda(x) + Q(x)\beta'(T^{*,\lambda}(x))u^\lambda(x) + 1 - r_1 u^\lambda(x) = 0, \quad u^\lambda|_{\partial\mathcal{D}} = 0.$$

Since $T^{*,\lambda}(x) \in (T_l, T_u)$ for all x and β is affine on (T_l, T_u) , we have $\beta'(T^{*,\lambda}(x)) \equiv s$. Hence

$$-\Delta u^\lambda(x) + (r_1 - Q(x)s)u^\lambda(x) = 1, \quad u^\lambda|_{\partial\mathcal{D}} = 0.$$

By (2.15) and the maximum principle, see [20, Section 6.4], it follows that

$$u^\lambda(x) > 0 \quad \text{in } \mathcal{D},$$

and in particular $u^\lambda(z_m) > 0$ for all interior grid points z_m .

Step 2: $\partial_\lambda f^\lambda > 0$ component-wise. Recall $f_m^\lambda = \beta(T^{*,\lambda}(z_m))$. Since $\beta'(T^{*,\lambda}(z_m)) \equiv s$,

$$\partial_\lambda f_m^\lambda = \beta'(T^{*,\lambda}(z_m)) \partial_\lambda T^{*,\lambda}(z_m) = s u^\lambda(z_m) > 0, \quad m = 1, \dots, d.$$

Also $f^\lambda > 0$ component-wise since $\beta \in (0, 1)$.

Step 3: K^λ is λ -independent on (T_l, T_u) . Because $\beta'(T^{*,\lambda}(z_m)) \equiv s$, we have $D^\lambda = sI$ and $B^\lambda = \text{diag}(-Q(z_m)s + r_1)$, hence D^λ, M^λ and K^λ do not depend on λ in this regime. We denote them simply by D, M and K .

Step 4: $-K$ is an irreducible nonsingular M -matrix and $(-K)^{-1} > 0$ entry-wise. Since A_Δ is the standard finite-difference Laplacian (five-point stencil) on a connected interior grid, its directed graph is strongly connected, hence A_Δ is irreducible. As B^λ is diagonal, $M^\lambda = A_\Delta - B^\lambda$ has the same off-diagonal pattern as A_Δ , so $-M$ is an irreducible Z -matrix. Consider the Kronecker sum

$$S := I_d \otimes (-M) + (-M) \otimes I_d.$$

Then S is a Z -matrix and is irreducible¹. Moreover, since D is diagonal, $D \otimes D$ is diagonal, hence $\text{diag}(\text{vec}(C))(D \otimes D)$ is diagonal. Therefore

$$-K = S - \tau \text{diag}(\text{vec}(C))(D \otimes D)$$

is still a Z -matrix and remains irreducible (diagonal modifications do not affect irreducibility). By assumption, K is negative definite, hence $-K$ is positive definite and in particular all eigenvalues of $-K$ have strictly positive real part. Since $-K$ is a Z -matrix, this implies that $-K$ is a nonsingular M -matrix. Together with irreducibility, it follows, thanks to [43, Corollary 3.8, Chapter 5], that

$$(-K)^{-1} > 0 \quad \text{entry-wise.}$$

Step 5: differentiate the stationary covariance formula and conclude strict positivity. By Lemma 2.5 and Corollary 2.6,

$$q_\infty^\lambda := \text{vec}(\Gamma_\infty^\lambda) = (-K)^{-1} F^\lambda, \quad F^\lambda = \tau \text{diag}(\text{vec}(C)) \text{vec}(f^\lambda (f^\lambda)^T).$$

Since K is constant in λ , differentiation gives

$$\partial_\lambda q_\infty^\lambda = (-K)^{-1} \partial_\lambda F^\lambda,$$

and

$$\partial_\lambda F^\lambda = \tau \text{diag}(\text{vec}(C)) \text{vec}((\partial_\lambda f^\lambda)(f^\lambda)^T + f^\lambda (\partial_\lambda f^\lambda)^T).$$

By Step 2, both f^λ and $\partial_\lambda f^\lambda$ are strictly positive component-wise, hence the matrix

$$G^\lambda := (\partial_\lambda f^\lambda)(f^\lambda)^T + f^\lambda (\partial_\lambda f^\lambda)^T$$

is strictly positive entry-wise, so $\text{vec}(G^\lambda) > 0$ component-wise. Since $C \geq 0$ entry-wise, $\text{diag}(\text{vec}(C)) \geq 0$ entry-wise, and because $C \neq 0$ we have $\text{diag}(\text{vec}(C)) \text{vec}(G^\lambda) \neq 0$. Therefore

$$\partial_\lambda F^\lambda \geq 0, \quad \partial_\lambda F^\lambda \neq 0.$$

Finally, since $(-K)^{-1} > 0$ entry-wise (Step 4), it follows that

$$\partial_\lambda q_\infty^\lambda = (-K)^{-1} \partial_\lambda F^\lambda > 0 \quad \text{component-wise,}$$

and hence $\partial_\lambda \Gamma_\infty^\lambda > 0$ entry-wise. \square

In particular, since the stationary spatial variance is the trace of Γ_∞^λ (see Definition 2.1), the previous result guarantees that it is monotone increasing with respect to λ .

¹Indeed, write the index set of \mathbb{R}^{d^2} as pairs (i, j) with $i, j \in \{1, \dots, d\}$. By definition of the Kronecker sum, S^λ allows moves that change *only one coordinate at a time*: from (i, j) to (i', j) whenever $(-M)_{ii'} \neq 0$, and from (i, j) to (i, j') whenever $(-M)_{jj'} \neq 0$. Since $-M$ is irreducible, its graph is strongly connected, hence any pair (i, j) can reach any other pair (i', j') by first moving in the i -coordinate and then in the j -coordinate. Therefore S is irreducible.

Corollary 2.8 (Monotonicity of the stationary spatial variance). *Under the assumptions of Proposition 2.7, the stationary spatial variance*

$$\text{Var}_{\text{sp},\infty}(\lambda) = \text{Tr}(\Gamma_\infty^\lambda)$$

is monotone increasing in λ .

Remark 2.9 (Stronger forcing, stronger climate spatial co-variability). *We remark that Proposition 2.7 states that*

$$\partial_\lambda(\Gamma_\infty^\lambda)_{ij} > 0 \quad \text{for all } i, j,$$

and therefore, for any two distinct grid points $z_i \neq z_j$,

$$\partial_\lambda \text{Cov}(Y_\infty^\lambda(z_i), Y_\infty^\lambda(z_j)) > 0.$$

In climate terms, increasing radiative forcing increase not only the amplitude of local fluctuations (variance or spatial variance) but also their spatial co-fluctuation: anomalies at different locations tend to move more “together” in the sense of increasing covariance.

This covariance-amplification effect is complementary to recent statistical work on sphere-cross-time temperature fields which studies temporal evolution (and possible non-stationarity) in the spherical-harmonic coefficients and develops rigorous change-point methodology; see, e.g., [9, 10, 39, 40]. These contributions focus on detecting departures from stationarity in observed data, while our result provides a forcing-driven mechanism producing monotone covariance amplification in a reduced stochastic EBM.

Note that among the assumptions of Proposition 2.7 there is $C = LL^T \geq 0$ element-wise. This is mandatory. Indeed, in the next example, we show that, if the spatial covariance matrix C of the noise has even one negative entry, then the monotonicity of the spatial variance may fail, even when the noise amplitude is increasing componentwise in λ .

Example 2.10 (Failure of monotonicity with negative correlations). *Consider the two-dimensional SDE with additive noise*

$$dY_t^\lambda = MY_t^\lambda dt + \Sigma^\lambda dW_t, \quad Y_0^\lambda = 0,$$

where W_t is a 2-dimensional Brownian motion and

$$\Sigma^\lambda := \text{diag}(f^\lambda)L, \quad C := LL^T.$$

We choose

$$M = \begin{pmatrix} -1 & s \\ s & -1 \end{pmatrix}, \quad 0 < s < 1,$$

so that M is symmetric negative definite (its eigenvalues are $-1 \pm s < 0$). Let

$$C = \begin{pmatrix} 1 & -c \\ -c & 1 \end{pmatrix}, \quad 0 < c < 1,$$

which is positive definite (its eigenvalues are $1 \pm c > 0$) but has a negative off-diagonal entry $C_{12} = -c < 0$. Let $L \in \mathbb{R}^{2 \times 2}$ such that $LL^T = C$; note that L exists, for instance, thanks to the Cholesky factorisation. Finally, define

$$f^\lambda = \begin{pmatrix} \lambda \\ 1 \end{pmatrix}, \quad \lambda \geq 0,$$

which is increasing componentwise in λ .

Let $\Gamma_t^\lambda := \mathbb{E}[Y_t^\lambda(Y_t^\lambda)^T]$. Since the noise is additive, Itô formula gives that Γ_t solves the ODE

$$\frac{d}{dt}\Gamma_t^\lambda = M\Gamma_t^\lambda + \Gamma_t^\lambda M^T + S^\lambda, \quad S^\lambda := \Sigma^\lambda(\Sigma^\lambda)^T.$$

Because $\Sigma^\lambda = \text{diag}(f^\lambda)L$ and $LL^T = C$, we have

$$S^\lambda = \text{diag}(f^\lambda)C \text{diag}(f^\lambda) = \begin{pmatrix} \lambda^2 & -c\lambda \\ -c\lambda & 1 \end{pmatrix}.$$

Since M is negative definite, Γ_t^λ converges to the unique stationary covariance Γ_∞^λ solving

$$M\Gamma_\infty^\lambda + \Gamma_\infty^\lambda M + S^\lambda = 0.$$

The stationary covariance matrix Γ_∞^λ can also be expressed as

$$\Gamma_\infty^\lambda = \int_0^\infty e^{Mu} S^\lambda e^{Mu} du.$$

Let $\sigma_+ := -1 + s$ and $\sigma_- = -1 - s$ be the eigenvalues, and let v_+, v_- be eigenvectors corresponding to respectively to σ_+ and σ_- . We can take them orthonormal and given by

$$v_+ = \frac{1}{\sqrt{2}} \begin{pmatrix} 1 \\ 1 \end{pmatrix}, \quad v_- = \frac{1}{\sqrt{2}} \begin{pmatrix} 1 \\ -1 \end{pmatrix}$$

Let

$$V := \begin{pmatrix} | & | \\ v_+ & v_- \\ | & | \end{pmatrix}$$

in such a way that $VV^T = V^T V = I$. Hence

$$V^T M V = \begin{pmatrix} -1 + s & 0 \\ 0 & -1 - s \end{pmatrix} := D_M.$$

Recall that

$$e^{Mu} = V e^{D_M u} V^T, \quad e^{D_M u} = \begin{pmatrix} e^{\sigma_+ u} & 0 \\ 0 & e^{\sigma_- u} \end{pmatrix}.$$

Using the linearity and cyclicity of the trace

$$\begin{aligned} \text{Tr}(\Gamma_\infty^\lambda) &= \text{Tr}\left(\int_0^\infty e^{Mu} S^\lambda e^{Mu} du\right) = \int_0^\infty \text{Tr}(e^{Mu} S^\lambda e^{Mu}) du = \int_0^\infty \text{Tr}(V e^{D_M u} V^T S^\lambda V e^{D_M u} V^T) du \\ &= \int_0^\infty \text{Tr}(V^T V e^{D_M u} V^T S^\lambda V e^{D_M u}) du \\ &= \int_0^\infty \text{Tr}(e^{D_M u} V^T S^\lambda V e^{D_M u}) du \\ &= \int_0^\infty \text{Tr}(e^{2D_M u} V^T S^\lambda V) du. \end{aligned}$$

Setting $\tilde{S}^\lambda := V^T S^\lambda V$, then

$$\text{Tr}(\Gamma_\infty^\lambda) = \int_0^\infty \text{Tr}(e^{2D_M u} \tilde{S}^\lambda) du = \int_0^\infty \left(e^{2u\sigma_+} \tilde{S}_{11}^\lambda + e^{2u\sigma_-} \tilde{S}_{22}^\lambda \right) du = -\frac{\tilde{S}_{11}^\lambda}{2\sigma_+} - \frac{\tilde{S}_{22}^\lambda}{2\sigma_-}.$$

Since

$$\tilde{S}_{11}^\lambda = \frac{\lambda^2 - 2c\lambda + 1}{2}, \quad \tilde{S}_{22}^\lambda = \frac{\lambda^2 + 2c\lambda + 1}{2},$$

we obtain, after some computations

$$\text{Tr}(\Gamma_\infty^\lambda) = \frac{\lambda^2 - 2cs\lambda + 1}{2(1 - s^2)}.$$

Computing the derivative with respect to λ , we observe that

$$\partial_\lambda \text{Tr}(\Gamma_\infty^\lambda) = \frac{\lambda - cs}{1 - s^2}.$$

Since $s \in (0, 1)$, for $\lambda < cs$ the spatial variance, i.e. the trace of the stationary covariance matrix, is decreasing.



FIGURE 1. Geographical distribution of the Arctic Ocean and its marginal seas. Numbered labels indicate: (1) Norwegian Sea, (2) Barents Sea, (3) Kara Sea, (4) Laptev Sea, (5) East Siberian Sea, (6) Chukchi Sea, (7) Beaufort Sea, (8) Baffin Bay, (9) Greenland Sea, and (10) Arctic Ocean.

3. ANALYSIS OF OBSERVATIONAL SEA SURFACE TEMPERATURE DATA

In this section we compare our results with data. The real-world data are the product of the net outcome of all the geophysical processes at work within the system and from this perspective, the model presented is highly simplified. We focus on Surface Sea Temperature (SST) during summer (August) in the northern high latitudes, above 60°N , where the ice-albedo feedback is predominant.

In glacial zones small temperature increments can trigger powerful feedbacks that further accelerate the initial warming. In particular, the ice-albedo feedback represents a key mechanism governing Arctic SST, especially during summer months [53]. When the temperature is near a certain threshold, a small temperature increase triggers ice melting, giving way to liquid water; since water has a much lower albedo, this leads to increased heat absorption and then to higher temperatures.

Due to the increase in CO_2 , Arctic regions are experiencing the so-called *Arctic Amplification* [50] and a severe retreat of sea ice [26]. Therefore, August SSTs are currently exhibiting higher values than in the past [11] and northern seas are undergoing a condition of abrupt interannual changes [33], leading to greater fluctuations in SST [1, 53]. This is the dynamic described by our model in Section 1.

Concerning Section 2, we addressed the concept of spatial variance. By this term, we intend to examine how the local mechanism described above manifests on a larger scale. This reflects the spatial uniformity of ice-water dynamics across the entire ocean, clarifying whether the process is homogeneous or characterised by a patchwork distribution [4, 52, 54]. In other words, we are assessing the heterogeneity of the phenomenon, looking at the extent to which the system is fragmented into patches, through the spatial variability of SST. In particular, we have shown that temperature variability, under a certain regime, also increases spatially, implying a patchy behaviour and non-homogeneous distribution.

We used observations from NOAA (National Oceanic and Atmospheric Administration), in particular NOAA OI SST V2 High Resolution Dataset (<https://psl.noaa.gov/data/gridded/data.noaa.oisst.v2.highres.html>), provided by the NOAA PSL, Boulder, Colorado, USA (<https://psl.noaa.gov>) [30]. The dataset employed to assess temporal variance analysis contains daily SST values from 1981/09 to 2026/01, with Spatial Coverage of 0.25 degree latitude x 0.25 degree longitude global grid (1440x720). For the spatial variance analysis, we utilised monthly mean SSTs, sharing the same timeframe and geographical extent as the aforementioned dataset.

Initially, to detect signals of temporal SST variability, we first fixed a study area. Then, we extracted data for every August between 1982 and 2025 and we computed the daily spatial mean for each selected month. Subsequently, we calculated statistics (histograms, mean, standard deviation) over overlapping 10-year periods (31×10 data for each period), moving the window forward by one year at a time.

In Figure 2 we show the case of the Kara Sea, a marginal sea of the Arctic Ocean. This example is consistent with our results. The top-left panel indicates the location of the study area. The top-right panel shows a comparison between the histograms of the spatial-averaged daily August SST for the first (blue) and the last (red) calculable decade, along with their respective mean and variance. We note that the distribution has evolved significantly over time: the mean is increased and the tails of the distribution have broadened, as confirmed by the increase in the mean value and standard deviation value, respectively. The bottom-left panel shows the decadal spatial mean of August SST over time (centred on the mid-year of each decade) and a significant increasing trend can be observed. The bottom-right panel shows the decadal spatial standard deviation of August SST over time (centred on the mid-year of each decade). After a stationary phase, also observable in the mean trend, a period of growth can be distinctly discerned, i.e. an increased variability. Similar observations can be done for Figure 3, which illustrates the Laptev Sea case [51].

Comparing the Arabic Sea (Figure 4) to the previous cases, the growth trend of the mean is considerably weaker and the distribution tails do not change in shape. Consequently, the standard deviation shows no growth and remains steady. This could possibly be explained by the fact that the equilibrium temperature of that area far exceeds the reference interval, meaning we are referring to the right-side plateau of the co-albedo curve (equation (1.2)), i.e. in (1.4) $\text{Var}'_{\infty} \equiv 0$.

Regarding the spatial variability of temperature, as mentioned before, we changed dataset. For each grid point within the study area, we used the August mean SST value to create a density map, where the colour intensity represents the frequency of SST values over time. We then calculated the standard deviation for each year, thus capturing the area's spatial spread, the fluctuations around the average value, i.e. its heterogeneity.

Figures 5 and 6 illustrate the spatial variability of the previously discussed seas, i.e. the Kara and Laptev Seas, respectively. The top panel shows the density map. In both cases, a clear widening of the spread is visible, indicating greater dispersion. The lower panel displays the interannual standard deviation, together with its growth trend (dashed red line), which is increasing.

In contrast to the aforementioned seas, the Arctic Ocean (panel 10, Figure 1) exhibits a different behaviour. As shown in Figure 7, the standard deviation remains stationary. This could possibly be explained by the fact that the average temperatures of those seas are still too low; that is, we are referring to the left-side plateau of the co-albedo curve (equation (1.2)), i.e. in (1.4) $\text{Var}'_{\infty} \equiv 0$. Indeed, persistent ice still characterises this area even during August.

ACKNOWLEDGMENTS

G.D.S. acknowledges the support from the DFG project FOR 5528. The research of F.F. is funded by the PRIN-PNRR project ‘‘Some mathematical approaches to climate change and its impacts’’ n. P20225SP98 and the European Union (ERC, NoisyFluid, No. 101053472). Views and opinions expressed are however those of the authors only and do not necessarily reflect those of the European Union or the European Research Council. Neither the European Union nor the granting authority can be held responsible for them. M.L. is supported by the the Italian national inter-university PhD course in Sustainable Development and Climate change. M.L. produced this work while attending the PhD programme in PhD in Sustainable Development And Climate Change at the University School for Advanced Studies IUSS

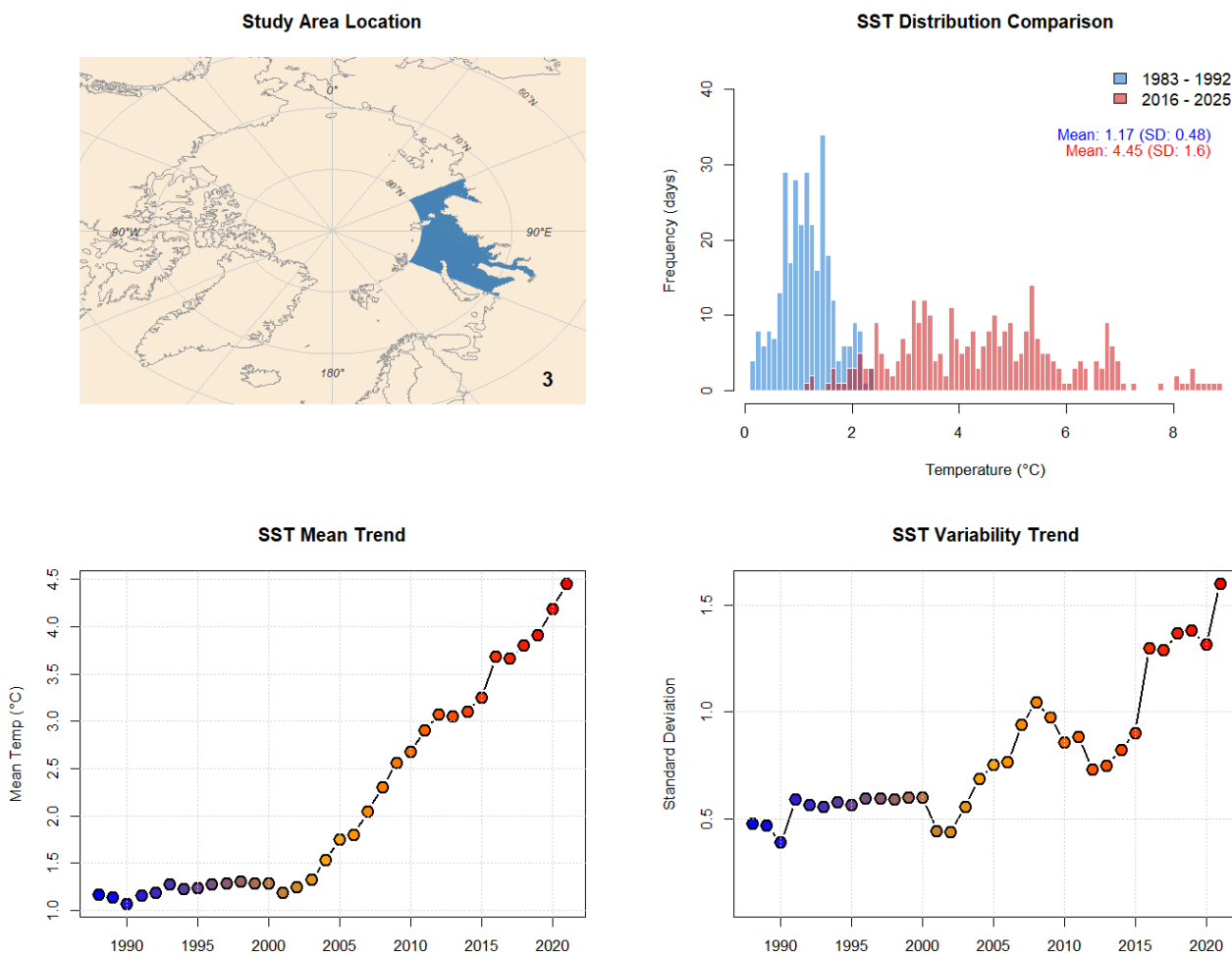


FIGURE 2. Kara Sea. Top-left: location of the study area. Top-right: comparison between the histograms (number of days) of the spatial-averaged daily August SST for the first decade (1983-1992, blue) and the last calculable decade (2016-2025, red), along with their respective mean and standard deviation values. Bottom-left: decadal spatial mean trend of August SST (centred on the mid-year of each decade, one year moving window). Bottom-right: decadal spatial standard deviation trend of August SST (centred on the mid-year of each decade, one year moving window). The blue-to-red colour scale represents the progression of time across the decades, in accordance with the colour scheme used in the histogram.

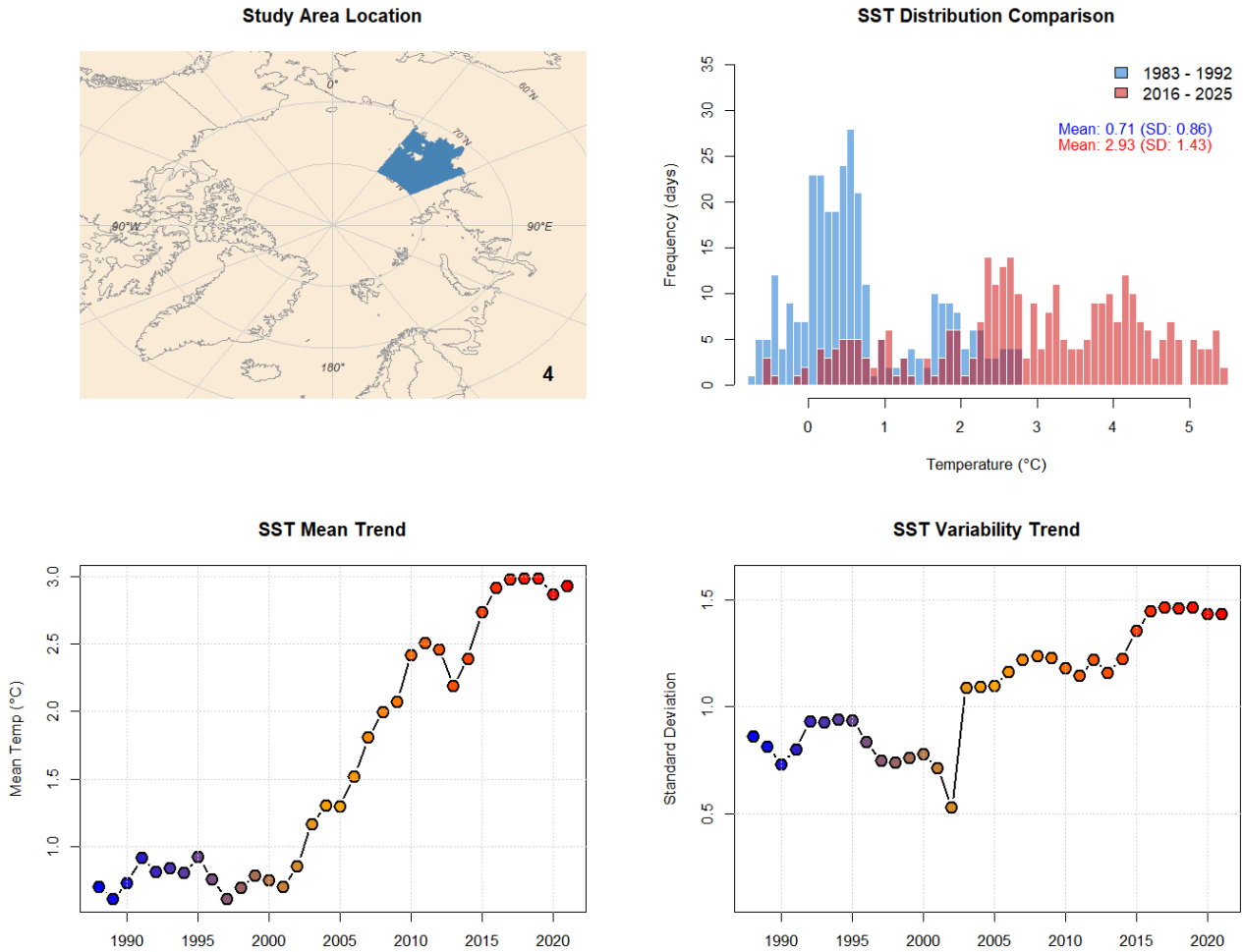


FIGURE 3. Laptev Sea. Top-left: location of the study area. Top-right: comparison between the histograms (number of days) of the spatial-averaged daily August SST for the first decade (1983-1992, blue) and the last calculable decade (2016-2025, red), along with their respective mean and standard deviation values. Bottom-left: decadal spatial mean trend of August SST (centred on the mid-year of each decade, one year moving window). Bottom-right: decadal spatial standard deviation trend of August SST (centred on the mid-year of each decade, one year moving window). The blue-to-red colour scale represents the progression of time across the decades, in accordance with the colour scheme used in the histogram.

REFERENCES

[1] M. Alexander, J. Scott, K. Friedland, J. Nye, M. Bender, D. Tommasi, C. Stock, and A. Marshak. Projected sea surface temperatures over the 21st century: Changes in the mean, variability and extremes for large marine ecosystem regions of Northern Oceans. *Elementa: Science of the Anthropocene*, 6(1):9, 2018.

[2] L. Arnold. Hasselmann’s program revisited: the analysis of stochasticity in deterministic climate models. In *Stochastic climate models*, volume 49, pages 141–157. Birkhäuser, Basel, 2001.

[3] P. Ashwin and A. Von der Heydt. Extreme sensitivity and climate tipping points. *Journal of Statistical Physics*, 179(5):1531–1552, 2020.

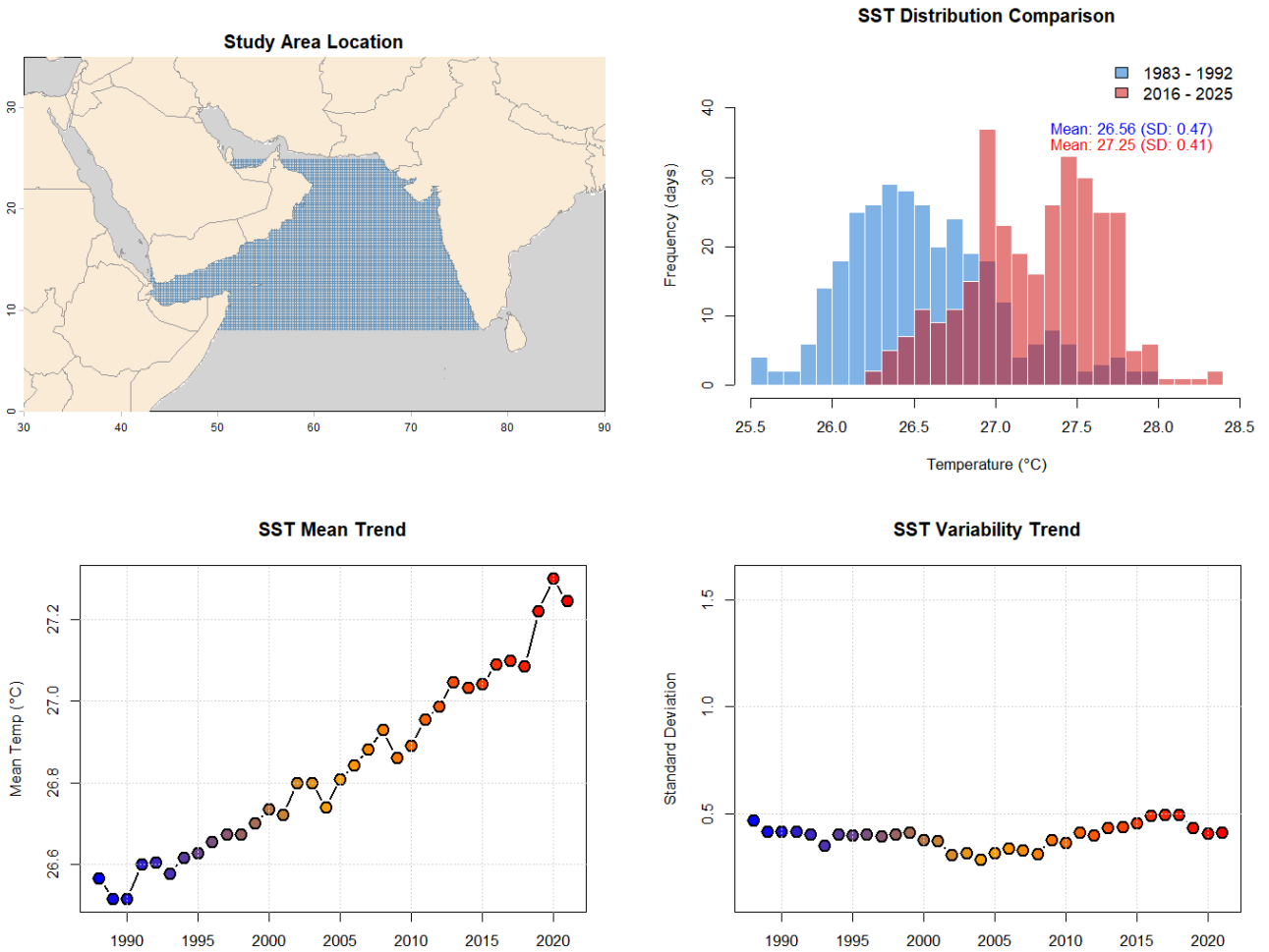


FIGURE 4. Arabi Sea. Top-left: location of the study area (long-lat). Top-right: comparison between the histograms (number of days) of the spatial-averaged daily August SST for the first decade (1983-1992, blue) and the last calculable decade (2016-2025, red), along with their respective mean and standard deviation values. Bottom-left: decadal spatial mean trend of August SST (centred on the mid-year of each decade, one year moving window). Bottom-right: decadal spatial standard deviation trend of August SST (centred on the mid-year of each decade, one year moving window). The blue-to-red colour scale represents the progression of time across the decades, in accordance with the colour scheme used in the histogram.

- [4] D. Barber, R. Galley, M. Asplin, R. De Abreu, K. Warner, M. Pucko, M. Gupta, S. Prinsenberg, and S. Julien. Perennial pack ice in the southern Beaufort Sea was not as it appeared in the summer of 2009. *Geophysical Research Letters*, 36(24):L24501, 2009.
- [5] R. Bastiaansen, H. Dijkstra, and A. von der Heydt. Fragmented tipping in a spatially heterogeneous world. *Environmental Research Letters*, 17(4):045006, mar 2022.
- [6] A. Berman and R. Plemmons. *Nonnegative matrices in the mathematical sciences*, volume 9. SIAM, 1994.
- [7] M. Budyko. The effect of solar radiation variations on the climate of the earth. *Tellus*, 21(5):611–619, 1969.
- [8] P. Cannarsa, V. Lucarini, P. Martinez, C. Urbani, and J. Vancostenoble. Analysis of a two-layer energy balance model: long time behavior and greenhouse effect. *Chaos*, 33(11):Paper No. 113111, 34, 2023.

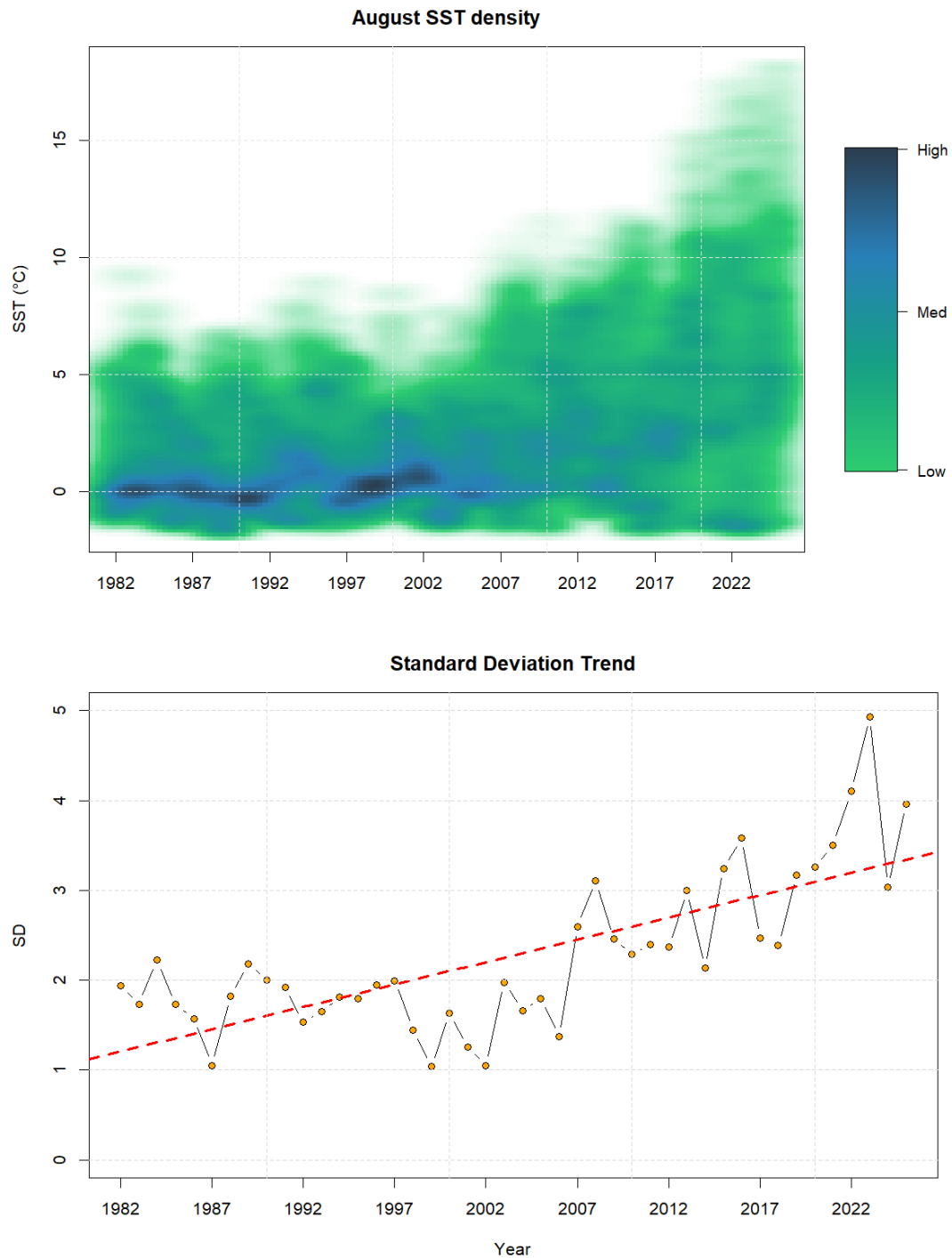


FIGURE 5. Kara Sea (panel 3, Figure 1). Top: density distribution of annual August mean SST values across all individual grid points of the study area. Bottom: interannual standard deviation (dashed line with markers), together with its growth trend (dashed red line).

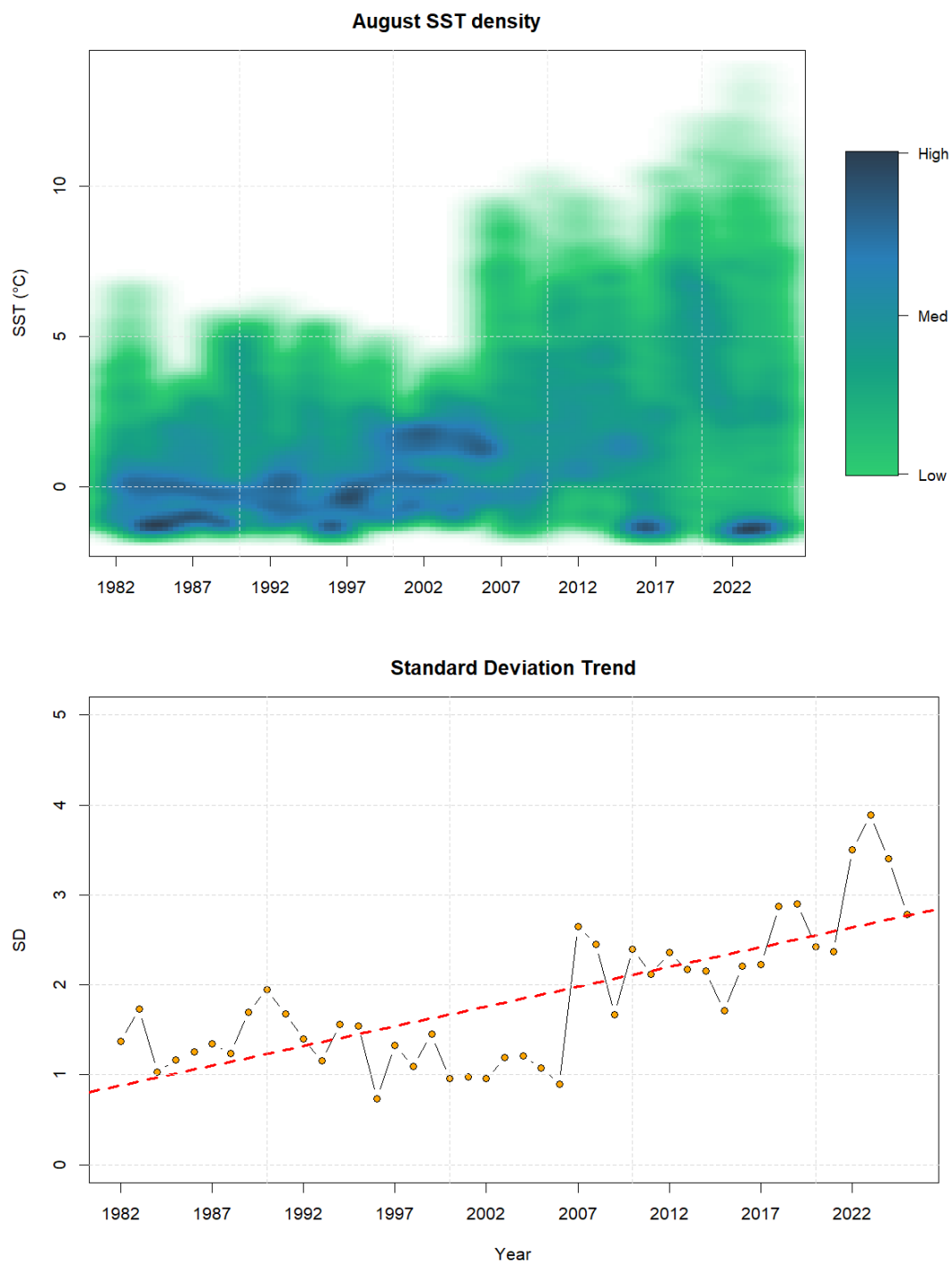


FIGURE 6. Laptev Sea (panel 4, Figure 1). Top: density distribution of annual August mean SST values across all individual grid points of the study area. Bottom: interannual standard deviation (dashed line with markers), together with its growth trend (dashed red line).

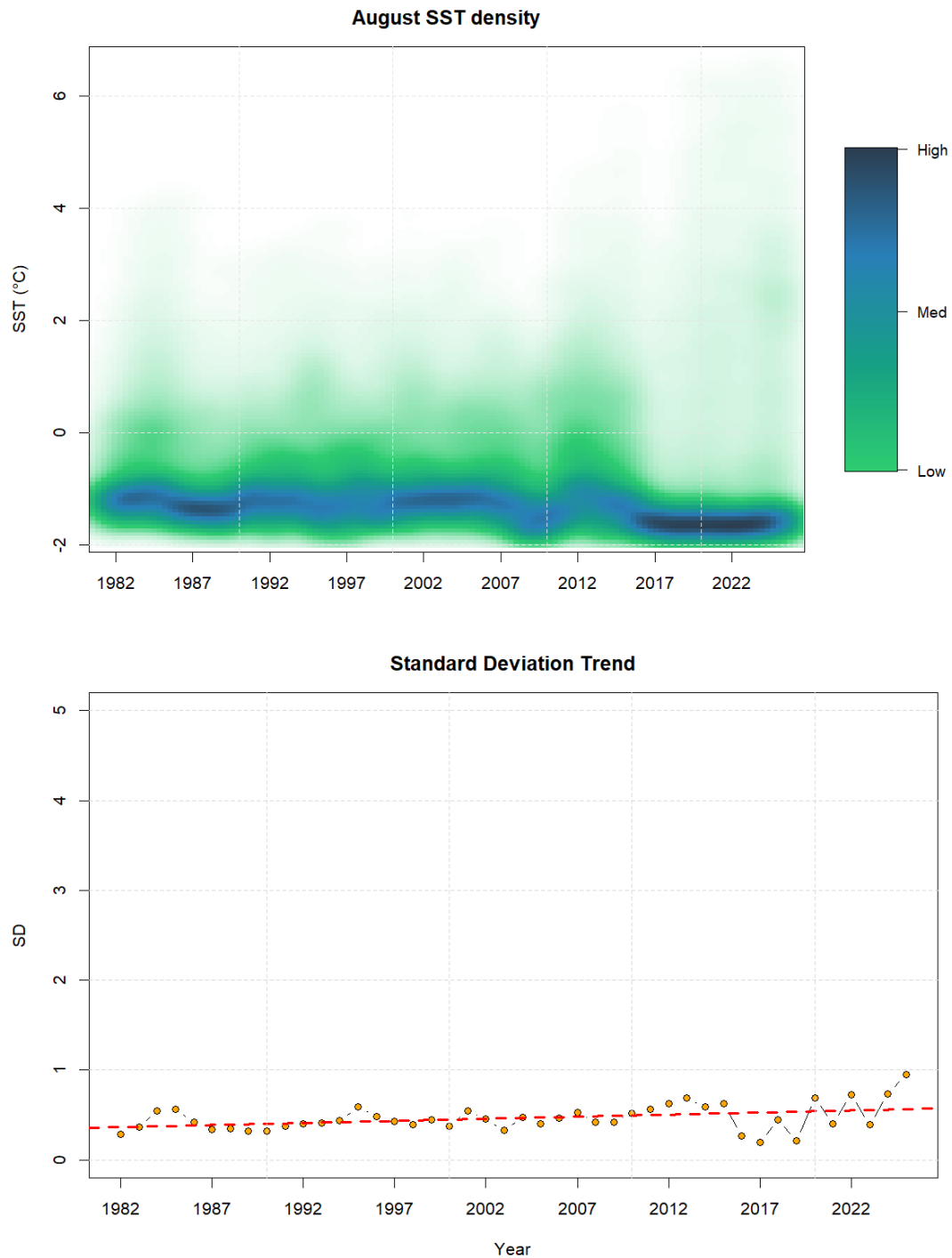


FIGURE 7. Arctic Ocean (panel 10, Figure 1). Top: density distribution of annual August mean SST values across all individual grid points of the study area. Bottom: interannual standard deviation (dashed line with markers), together with its growth trend (dashed red line).

- [9] A. Caponera and D. Marinucci. Asymptotics for spherical functional autoregressions. *Ann. Statist.*, 49(1):346–369, 2021.
- [10] A. Caponera, D. Marinucci, and A. Vidotto. Multi-Scale CUSUM tests for time dependent spherical random fields. *arXiv preprint arXiv:2305.01392*, 2023.
- [11] K. Carvalho and S. Wang. Sea surface temperature variability in the Arctic Ocean and its marginal seas in a changing climate: Patterns and mechanisms. *Global and Planetary Change*, 193:103265, 2020.
- [12] G. Da Prato and J. Zabczyk. *Stochastic equations in infinite dimensions*, volume 152. Cambridge University Press, Cambridge, second edition, 2014.
- [13] G. Del Sarto, J. Bröcker, F. Flandoli, and T. Kuna. Variational techniques for a one-dimensional energy balance model. *Nonlinear Processes in Geophysics*, 31(1):137–150, 2024.
- [14] G. Del Sarto, M. Hieber, F. Palma, and T. Zöchling. Time-periodic solutions to an energy balance model coupled with an active fluid under arbitrarily large forces. *Nonlinear Analysis: Real World Applications*, 90:104558, 2026.
- [15] G. Del Sarto, M. Hieber, and T. Zöchling. Dynamic boundary conditions with noise for an energy balance model coupled to geophysical flows. *Mathematische Nachrichten*, 299(1):60–84, 2026.
- [16] J. Díaz. On the mathematical treatment of energy balance climate models. In *The mathematics of models for climatology and environment*, volume 48 of *NATO ASI Ser. I Glob. Environ. Change*, pages 217–251. Springer, Berlin, 1997.
- [17] B. Dortmans, W. Langford, and A. Willms. An energy balance model for paleoclimate transitions. *Climate of the Past*, 15(2):493–520, 2019.
- [18] I. Eisenman. Factors controlling the bifurcation structure of sea ice retreat. *Journal of Geophysical Research: Atmospheres*, 117(D1), 2012.
- [19] I. Eisenman and J. Wettlaufer. Nonlinear threshold behavior during the loss of arctic sea ice. *Proceedings of the National Academy of Sciences*, 106(1):28–32, 2009.
- [20] L. Evans. *Partial differential equations*, volume 19. American mathematical society, 2022.
- [21] G. Floridia. Nonnegative controllability for a class of nonlinear degenerate parabolic equations with application to climate science. *Electron. J. Differential Equations*, pages Paper No. 59, 27, 2020.
- [22] F. Fornasaro, T. Kuna, and G. Carigi. Well-posedness and long time dynamics for a quasi-geostrophic ocean-atmosphere model with radiation balance. *arXiv preprint arXiv:2512.19556*, 2025.
- [23] M. Ghil. Climate stability for a sellers-type model. *Journal of Atmospheric Sciences*, 33(1):3 – 20, 1976.
- [24] M. Ghil and V. Lucarini. The physics of climate variability and climate change. *Rev. Mod. Phys.*, 92:035002, Jul 2020.
- [25] P. Goodwin and R. Williams. On the arctic amplification of surface warming in a conceptual climate model. *Physica D: Nonlinear Phenomena*, 454:133880, 2023.
- [26] H. Goosse, O. Arzel, C. M. Bitz, A. de Montety, and M. Vancoppenolle. Increased variability of the Arctic summer ice extent in a warmer climate. *Geophysical Research Letters*, 36(23):L23702, 2009.
- [27] A. Hall. The role of surface albedo feedback in climate. *Journal of Climate*, 17(7):1550 – 1568, 2004.
- [28] K. Hasselmann. Stochastic climate models part I. Theory. *Tellus*, 28(6):473–485, 1976.
- [29] J. Houghton, Y. Ding, D. Griggs, M. Noguer, P. van der Linden, X. Dai, K. Maskell, and C. Johnson, editors. *Climate Change 2001: The Scientific Basis*. Contribution of Working Group I to the Third Assessment Report of the Intergovernmental Panel on Climate Change, 2001.
- [30] B. Huang, C. Liu, V. Banzon, E. Freeman, G. Graham, B. Hankins, T. Smith, and H.-M. Zhang. Improvements of the Daily Optimum Interpolation Sea Surface Temperature (DOISST) Version 2.1. *Journal of Climate*, 34(8):2923–2939, 2021.
- [31] N. Ikeda and S. Watanabe. *Stochastic differential equations and diffusion processes*, volume 24. North-Holland Publishing Co., Amsterdam-New York; Kodansha, Ltd., Tokyo, 1981.
- [32] I. Karatzas and S. Shreve. *Brownian motion and stochastic calculus*, volume 113 of *Graduate Texts in Mathematics*. Springer-Verlag, New York, second edition, 1991.
- [33] L. Landrum and M. M. Holland. Extremes become routine in an emerging new Arctic. *Nature Climate Change*, 10(12):1106–1110, 2020.
- [34] R. LeVeque. *Finite difference methods for ordinary and partial differential equations*. SIAM, 2007.
- [35] S. Lewis and A. King. Evolution of mean, variance and extremes in 21st century temperatures. *Weather and Climate Extremes*, 15:1–10, 2017.
- [36] G. Lohmann. Temperatures from energy balance models: The effective heat capacity matters. *Earth System Dynamics*, 11(4):1195–1208, 2020.
- [37] I. Longo, R. Obaya, and A. Sanz. Nonautonomous modelling in energy balance models of climate. limitations of averaging and climate sensitivity. *Physica D: Nonlinear Phenomena*, 485:135038, 2026.
- [38] V. Lucarini, L. Serdukova, and G. Margazoglou. Lévy noise versus gaussian-noise-induced transitions in the ghil–sellers energy balance model. *Nonlinear Processes in Geophysics*, 29(2):183–205, 2022.
- [39] D. Marinucci, M. Rossi, and A. Vidotto. Non-universal fluctuations of the empirical measure for isotropic stationary fields on $S^2 \times \mathbb{R}$. *Ann. Appl. Probab.*, 31(5):2311–2349, 2021.
- [40] D. Marinucci, M. Rossi, and A. Vidotto. Fluctuations of level curves for time-dependent spherical random fields. *Ann. H. Lebesgue*, 7:583–620, 2024.
- [41] G. North, R. Cahalan, and J. Coakley. Energy balance climate models. *Reviews of Geophysics*, 19(1):91–121, 1981.

- [42] G. North and K. Kim. *Energy balance climate models*. Wiley Series in Atmospheric Physics and Remote Sensing". John Wiley & Sons, 2017.
- [43] R. Plemmons. M -matrix characterizations. I. Nonsingular M -matrices. *Linear Algebra and its applications*, 18(2):175–188, 1977.
- [44] A. Quarteroni. *Numerical models for differential problems*, volume 16 of *MS&A. Modeling, Simulation and Applications*. Springer, Cham, third edition, 2017.
- [45] J. Rombouts and M. Ghil. Oscillations in a simple climate–vegetation model. *Nonlinear Processes in Geophysics*, 22(3):275–288, 2015.
- [46] B. Rose and J. Marshall. Ocean heat transport, sea ice, and multiple climate states: Insights from energy balance models. *Journal of the Atmospheric Sciences*, 66(9):2828 – 2843, 2009.
- [47] S. Särkkä and A. Solin. *Applied stochastic differential equations*, volume 10 of *Institute of Mathematical Statistics Textbooks*. Cambridge University Press, Cambridge, 2019.
- [48] W. Sellers. A global climatic model based on the energy balance of the earth-atmosphere system. *Journal of Applied Meteorology and Climatology*, 8(3):392–400, 1969.
- [49] S. Seneviratne, X. Zhang, M. Adnan, W. Badi, C. Dereczynski, A. Di Luca, I. Pinto, M. Magnuson, J. Iturbide, N. Küttel, G. Kurten, B. J. Lall, R. Libonati, A. Martens, C. Stevens, and R. Vautard. *Weather and Climate Extreme Events in a Changing Climate*, pages 1513–1766. Cambridge University Press, 2021.
- [50] M. Serreze and R. Barry. Processes and impacts of arctic amplification: A research synthesis. *Global and Planetary Change*, 77(1):85–96, 2011.
- [51] P. Shabanov, A. Osadchiv, N. Shabanova, and S. Ogorodov. Decline in Ice Coverage and Ice-Free Period Extension in the Kara and Laptev Seas during 1979–2022. *Remote Sensing*, 16(11):1875, 2024.
- [52] C. Strong and I. Rigor. Arctic marginal ice zone trending wider in summer and narrower in winter. *Geophysical Research Letters*, 40(18):4864–4868, 2013.
- [53] M. Timmermans and Z. Labe. Sea Surface Temperature. NOAA Technical Report OAR ARC 23-07, National Oceanic and Atmospheric Administration (NOAA), 2023. In: Arctic Report Card 2023.
- [54] M.-L. Timmermans. The impact of stored solar heat on Arctic sea ice growth. *Geophysical Research Letters*, 42(15):6399–6406, 2015.
- [55] K. Twardowska. Wong-Zakai approximations for stochastic differential equations. *Acta Appl. Math.*, 43(3):317–359, 1996.
- [56] R. van de Wal and J. Oerlemans. An energy balance model for the greenland ice sheet. *Global and Planetary Change*, 9(1):115–131, 1994.
- [57] N. Watkins, R. Calel, S. Chapman, A. Chechkin, R. Klages, and D. Stainforth. The challenge of non-markovian energy balance models in climate. *Chaos: An Interdisciplinary Journal of Nonlinear Science*, 34(7):072105, 07 2024.
- [58] M. Winton. Amplified arctic climate change: What does surface albedo feedback have to do with it? *Geophysical Research Letters*, 33(3), 2006.

TECHNISCHE UNIVERSITÄT DARMSTADT, FACHBEREICH MATHEMATIK, SCHLOSSGARTENSTR. 7, 64289 DARMSTADT, GERMANY,

Email address: `delsarto@mathematik.tu-darmstadt.de`

SCUOLA NORMALE SUPERIORE, CLASSE DI SCIENZE, P.ZA DEI CAVALIERI 7, 56126 PISA, ITALY

Email address: `franco.flandoli@sns.it`

SCUOLA NORMALE SUPERIORE, CLASSE DI SCIENZE, P.ZA DEI CAVALIERI 7, 56126 PISA, ITALY

Email address: `marta.lenzi@sns.it`

UNIVERSITY SCHOOL FOR ADVANCED STUDIES IUSS PAVIA, DEPARTMENT OF SCIENCE, TECHNOLOGY AND SOCIETY, P.ZA DELLA VITTORIA 15, 27100 PAVIA, ITALY

Email address: `marta.lenzi@iusspavia.it`